Eur. Phys. J. C (2024) 84:167
https://doi.org/10.1140/epjc/s10052-024-12488-0

THE EUROPEAN PHYSICAL JOURNAL C

Regular Article - Theoretical Physics

Theoretical priors and the dark energy equation of state

Ido Ben-Dayan, Utkarsh Kumar[a]

Physics Department, Ariel University, Ariel 40700, Israel

Received: 22 October 2023 / Accepted: 28 January 2024 / Published online: 19 February 2024

Abstract We revisit the theoretical priors used for inferring Dark Energy (DE) parameters. Any DE model must have some form of a tracker mechanism such that it behaved as matter or radiation in the past. Otherwise, the model is fine-tuned. We construct a model-independent parametrization that takes this prior into account and allows for a relatively sudden transition between radiation/matter to DE behavior. We match the parametrization with current data, and deduce that the adiabatic and effective sound speeds of DE play an important role in inferring the cosmological parameters. We find that there is a preferred transition redshift of $1+z \simeq 29-30$, and some reduction in the Hubble and Large Scale Structure tensions.

1 Introduction

The standard Λ cold dark matter model (ΛCDM), also known as the Concordance Model, is a well-established cosmological model supported by data from numerous observations. Combining various observations such as the cosmic microwave background (CMB) measurements [1–3], supernovae type Ia [4], weak lensing [5–8], and galaxy clustering measurements [9–17] the ΛCDM parameters have been constrained to about a percent accuracy.

From a historical perspective, the last parameter that was accepted by the scientific community into the Concordance Model, was the cosmological constant, Λ. The presence of a dominant positive cosmological constant explains the present acceleration of the Universe, with its relative energy density being $\Omega_\Lambda \simeq 0.70$. Another property of a true cosmological constant should manifest itself in observations of an equation of state (eos) with the value of $w = -1$. Considering a constant eos without imposing $w = -1$, the data further constrains the eos to be $-1.14 < w < -0.94$ [2,18].[1] A true constant, based on zero modes quantum fluctuations of the fields present in Nature, is expected to be many orders of magnitude above the observed value and there have been many attempts to reconcile the measurement with the theoretical expectation [19–29]. This unappealing mismatch between theory and observations prompted the idea that the present acceleration is due to an evolving (usually scalar) field, dubbed Dark Energy (DE) [30,31]. Generically, this scalar field is not solving the so-called "old" cosmological constant problem (of the expected zero modes contribution to the energy density of the Universe). Nevertheless, assuming this question is somehow settled, DE gives predictions for the present acceleration of the Universe.

If DE is realized in Nature then generically the eos is time or redshift dependent $w(z)$. Furthermore, the DE fluid/field will have fluctuations that will affect the growth of structure [32–35], thus providing a testable framework. Focusing on the eos, there are many possible parametrizations [36–44], perhaps most notably the CPL parametrization [36,37]

$$w(z) \simeq w_0 + w_1 \frac{z}{1+z}, \tag{1}$$

which is not valid at all redshifts. Combining Planck with BAO and Supernovae data then gives $w_0 = -0.957 \pm 0.080$, $w_1 = -0.29^{+0.32}_{-0.26}$ [2]. Since DE is evolving with time, another tuning problem arises – why should its energy density and eos be such that it behaves nearly as a cosmological constant today [45–47]? To avoid this coincidence, DE models are generically endowed with a tracker mechanism. The DE tracks the radiation or matter throughout the evolution of the Universe, until it decouples and acts as DE today [48,49]. We would like to include this theoretical prior into the parameter estimation analysis.

[a] e-mail: kumarutkarsh641@gmail.com (corresponding author)

[1] This model is usually dubbed wCDM.

On top of the theoretical difficulties, despite its remarkable success, the validity of the Concordance Model is currently under investigation, as accumulation of data results in tensions between various measurements. Specifically, the values of some cosmological parameters of ΛCDM inferred from different cosmological and astrophysical data are in tension with Planck 2018 results, [2]. Perhaps the most intriguing tensions are the Hubble H_0 tension and Large Scale Structure (LSS) or so-called S_8 tension. The Hubble tension arises from the discrepancy in the measurement of the present value of the Hubble parameter H_0 between model-dependent and model-independent probes. Most notably, there is a $\sim 5\sigma$ discrepancy between the SH0ES result, that is model-independent, [50–63] and Planck 2018 CMB measurements, that are model dependent, [2]. Considering additional measurements, the various data sets can be divided roughly into Early Universe and Late Universe probes see [64] and references therein. Thus, the discrepancy in H_0 persists with lower values for the Early Universe probes, and a higher value for the Late Universe probes.

$S_8 = \sigma_8\sqrt{\Omega_m/0.3}$ is a parameter measuring linear fluctuations, where σ_8 is the amplitude of linear fluctuations smoothed over 8 Mpc h^{-1}, and Ω_m is the relative matter density today. In inferring S_8 there again seems to be a $2-3\sigma$ discrepancy between Planck and Weak Lensing experiments, e.g. [2,65–73], leading to the S_8 or LSS tension. Various solutions have been proposed to solve both tensions individually [31,53,54,58,64–71,73–147]. Some solutions resolving the Hubble tension seem to worsen the LSS tension and vice-versa [35,90,124–126,148]. A theory that addresses both of these conflicts at once would undoubtedly be appealing, so in this study we make a point of attempting to handle the S_8 and H_0 tensions concurrently [149–151].

Recently, we have suggested an emerging DE model. In this model the DE is not a fundamental scalar field, but rather a thermodynamical collective behavior [149–151]. This approach solves the fine tuning and initial conditions problems, is free of the swampland conjectures [152–159] and does not modify gravity. The model has a built-in tracker mechanism since it asymptotes to $w = -1$ at future infinity and to $w = 1/3$ in the past – i.e. the fluid behaves as radiation in the past and transitions to DE behavior at some redshift. Our recent analysis shows that the model is restoring cosmological concordance and alleviating both the Hubble tension and the S_8 tension, performing significantly better than ΛCDM [149]. Motivated by this success, we want to investigate whether this behavior is more generic.

Since any valid DE model has $w(z = 0) \simeq -1$ and any model with a tracker mechanism $w(z \gg 1) = 1/3\, or\, 0$, we can implement this understanding into our parametrization. We can then test the novel parametrization and its effect on existing tensions such as the Hubble or S_8 tensions. We consider DE to be some phenomenological fluid, and develop a phenomenological approach where the eos of the fluid at the most economical level is:

$$w_{DE}(a) = -1 + \frac{w_a}{1 + (a/a_t)^n}, \tag{2}$$

where n is some integer, a_t is a transition scale factor around which w_{DE} transitions from $w_{DE} \simeq -1$ to $w_{DE} \simeq -1+w_a$. To demonstrate our approach, we shall consider the possibility $w_a = 4/3$, such that the DE behaves as radiation at early times. Thus, the parameter that has to be inferred from measurements is neither w_0 nor w_a, but rather the transition redshift/scale factor a_t. In this minimal approach c_s^2 is determined, so we are fitting less parameters that the usual CPL parametrization. We then extend our model to include c_s and later also n as a free parameters. We calculate the background and perturbations evolution and match to existing data. We then perform a likelihood analysis of our model combining various data sets. We find some modest reduction in the Hubble and S_8 tension and some reduction in $\Delta\chi^2 \sim -2-3$ compared to ΛCDM. The more interesting result is that we find the transition redshift to be highly constrained, $z_t = 29-30$, providing a definite interval for exploration.

Our model belongs to the category of fast transition dark energy models, as discussed in previous works [160–163], where transition redshifts were considered within the range of [1, 5]. However, our analysis sets itself apart by conducting a rigorous likelihood analysis, incorporating diverse cosmological data, and addressing the microphysics of the dark energy fluid. Consequently, our findings diverge from those of previously explored models.

The paper is organized as follows. We first describe the background and perturbation evolution of our proposed phenomenological fluid parametrization in Sect. 2. In Sect. 3 we discuss the different data sets and methods used to analyze our proposed parametrization. This section also includes the nomenclature of the different models. We report our results in Sect. 4, and we finally conclude in Sect. 5.

2 Phenomenological fluid dark energy

We propose a scenario consisting of the standard cosmological model with cold dark matter (CDM) and DE using a phenomenological fluid with several critical key features which differ from the cosmological constant (CC). In this section will discuss the model, its background, and perturbative dynamics. Using our approach, we also illustrate the implications on cosmological tensions such as Hubble, H_0, and Large Scale Structure, S_8.

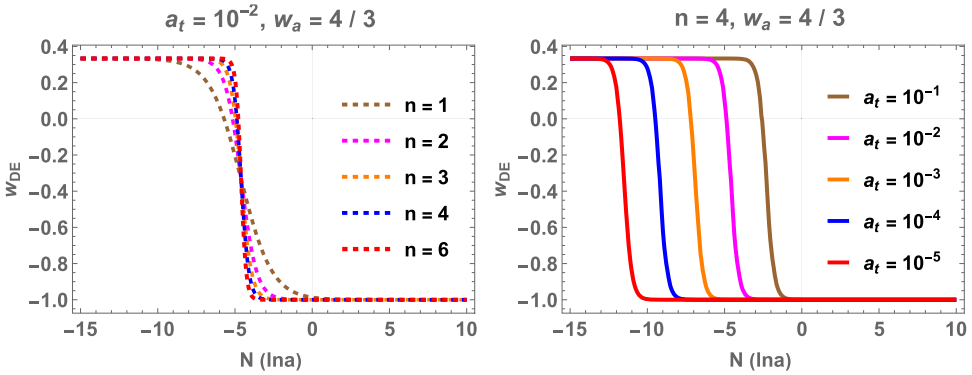

Fig. 1 Evolution of dark energy equation of state w_{DE} as a function of e-folds, $N = \ln a$, for different values of n and a_t while fixing other parameters in left and right panels respectively. $N = 0$ corresponds to today

2.1 Theory

Our proposed scenario mimics Λ, which is used to account for Dark Energy in late times and transits to radiation at early times. The model is specified by a time-varying equation of state for such phenomenological fluid.

Conditions of DE model We start our discussion by pointing out the conditions for a successful Dark Energy Model as

- The Dark Energy model should be able to explain cosmic coincidence and the hierarchy problem of DE, e.g., Λ.
- There should be an era of dust domination, which is essential for the structure of the Universe.
- The equation of state of DE component today, defined as $w_{DE} = \frac{p_{DE}}{\rho_{DE}}$ where ρ_{DE} and p_{DE} being the energy density and pressure of the DE fluid respectively, must lie within $-1.14 < w_{DE} < -0.94$ [2,18].
- The evolution of DE fluid and hence the whole background and perturbative evolution of the Universe should be free from instability. Thus, there should be no gradient instability and the sound speed of DE fluid should be subluminal, i.e., $0 < c^2_{DE,a} < 1$. Here $c^2_{DE,a} = \frac{\dot{p}_{DE}}{\dot{\rho}_{DE}}$ is the squared sound speed of DE fluid.

Background The time-varying eos of a phenomenological fluid (w_{DE}) is governed by the following form

$$w_{DE}(a) = -1 + \frac{w_a}{1 + (a/a_t)^n}, \tag{3}$$

where we normalize the scale factor a to be unity today. Equation (3) asymptotes to $w_{DE}(a) = -1 + w_a$ and $w_{DE}(a) = -1$ at early and late times respectively. w_a tunes the desired eos of state of the Dark Energy fluid at early times, and a_t is the "transition scale factor" or redshift at which the fluid approximately crosses $w_{DE} = 0$. The parameter n controls the sharpness of this transition. Using the equation (3), it is straightforward to derive the energy density of the fluid as

$$\rho_{DE}(a) = \rho_{DE,0}\, a^{-3\,w_a} \left(\frac{1 + (a/a_t)^n}{1 + (1/a_t)^n}\right)^{3\,w_a/n}. \tag{4}$$

Equations (3) and (4) give us a full picture of the background for our Dark Energy model as a phenomenological fluid with up to 3 parameter extension compared to ΛCDM.

Our proposal for Dark Energy using **P**henomenological **F**luid **D**ark **E**nergy (PFDE) has a built-in tracker mechanism that tracks the background throughout evolution. Since we would like the PFDE to track the background evolution of the Universe as a whole, we require that the eos of phenomenological fluid will lie within $\in [0, 1/3]$ at early times, which constrains w_a as

$$w^{Early}_{DE} \approx -1 + w_a \in [0, 1/3] \Rightarrow w_a \in [1, 4/3] \tag{5}$$

We think the new parametrization has several advantages over existing ones: First, it captures the essence of DE with $w \simeq -1$. Second, it captures the tracker behavior of $w = 1/3$ at large redshift. Third, there is a single free parameter – the transition redshift or scale factor a_t. Thus, in terms of the number of cosmological parameters it is equivalent to wCDM with fixed w. Later, when we allow for an arbitrary c^2_s, we have the same number of parameters as the CPL one, but with different theoretical input.

Let us demonstrate the behavior of the model. First, we present examples of the effect of the steepness of transition and transition redshift on the DE eos w_{DE} in Fig. 1. It is clear from the plots that w_{DE} transits from $1/3$ to -1, with different transition steepness (from varying n) and at different transition redshifts (varying a_t), at early and late times.

Next, we discuss the evolution of the effective eos of the Universe, w_{tot}. There is almost no difference from the standard ΛCDM for different values n while there is a strong dependence of w_{tot} on a_t, as shown in the left and right panel of Fig. 2. It is evident from the right panel of Fig. 2, that as we increase the value of a_t, DE+radiation dominate over the matter sector and we see no era of dust domination which

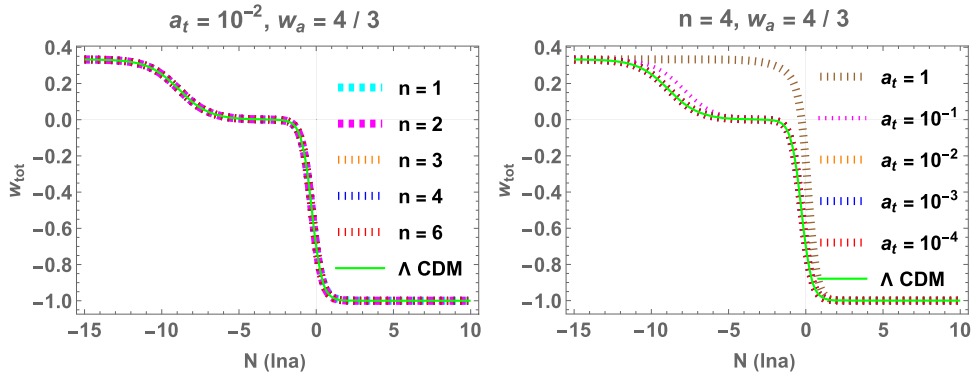

Fig. 2 Evolution of total equation of state (w_{tot}) as a function of e-folds, $N = \ln a$, for different values of n and a_t while fixing other parameters in left and right panels respectively

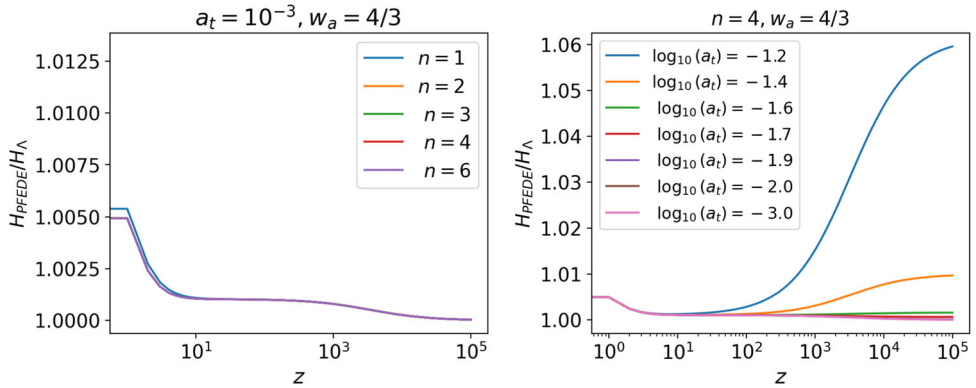

Fig. 3 Comparison of the expansion rate of PFDE model and ΛCDM using their best fir parameters inferred from all data sets. We plot H_{PFDE}/H_0 with varying n and a_t on the left and right panels respectively

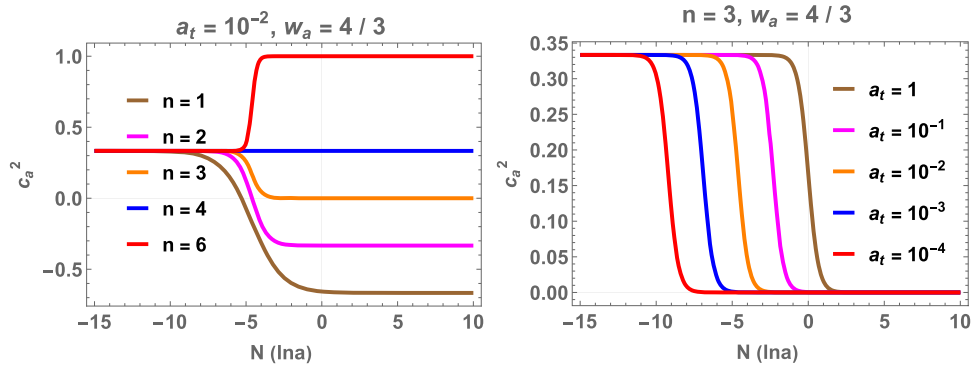

Fig. 4 The evolution of the adiabatic sound speed c_a^2 for PFDE model parameters. The left panel shows that the adiabatic sound speed becomes negative at late times for $n < 3$. The right panel illustrates the transition of c_a^2 for different values of a_t

is crucial for structure formation. Thus, we limit $a_t \leq 0.1$. Finally, we compare the expansion rate of PFDE model and ΛCDM using the best fit model parameters inferred from the combination of all data sets. To appreciate the increase in expansion rate in our model, we present our results normalized with respect to the expansion rate of ΛCDM. In the left and right panel of Fig. 3, we show the dependence of H_{PFDE}/H_Λ on n and a_t respectively. In all cases the inferred Hubble parameter in the PFDE model is larger than the ΛCDM one.

Perturbations The evolution of perturbations depends on the sound horizon of DE. In the FLRW Universe, the sound horizon of DE with effective sound speed c_s is defined as

$$r_s(\eta) = \int \frac{c_s}{a\,\mathcal{H}}\, d\eta, \tag{6}$$

where $\mathcal{H}(\equiv a'/a)$ is the conformal Hubble constant, and $'$ denotes derivative with respect to conformal time η. Depending on the properties of the fluid, it will have different clustering effects, and c_s plays crucial role in the evolution of DE perturbation. If c_s is close to unity, DE perturbations are suppressed by pressure. As a result DE does not cluster except on scales comparable to r_s. In the case of $c_s \ll 1$, DE starts clustering as a dark matter component with the consequence of affecting matter perturbations. Finally, considering a more general effective speed of sound $0 \leq c_s^2 \leq 1$, for example from non-canonical scalar fields or unparticles, can result in different forms of clustering [149–151].[2]

Any phenomenological fluid is characterized by the energy density ρ_{DE}, pressure p_{DE}, momentum density, and anisotropic stress σ_{DE}. The pressure δp_{DE} and energy density perturbations $\delta\rho_{DE}$ are related by the effective sound speed which is gauge dependent quantity $c_s^2 = \frac{\delta p_{DE}}{\delta \rho_{DE}}$. For canonical scalar field models, it is automatically set to unity. To avoid such gauge ambiguities, we consider the gauge invariant formulation of pressure perturbations in Fourier space allowing for a general effective sound speed as discussed in [164].

$$\delta p_{DE} = c_s^2\,\delta\rho_{DE} + 3\,\mathcal{H}\left(c_s^2 - c_a^2\right) (1+w_{DE})\,\rho_{DE}\,\theta_{DE}/k^2. \tag{7}$$

Here θ_{DE} is the velocity divergence, and c_a^2 is the adiabatic sound speed for our phenomenological fluid, which takes the following form

$$c_a^2 \equiv w_{DE} - \frac{w'_{DE}}{3\,\mathcal{H}\,(1+w_{DE})} = w_{DE} - \frac{n}{3\,w_a}\,(1+w_{DE}-w_a)\,, \tag{8}$$

where for $w_a = 4/3$ we have $c_a^2 = w_{DE}(1-\frac{n}{4}) + \frac{n}{12}$. The adiabatic sound speed and its dependence on the model parameters are depicted in Fig. 4. Notice that for $n < 3$ the adiabatic speed of sound tends to negative values, raising the danger of instabilities. We will see that even without addressing this theoretical issue, the data will prefer $n \geq 3$.

We write the perturbation equations in synchronous gauge with the following line element:

$$d\,s^2 = a^2(\eta)\left[-d\,\eta^2 + \left(\eta_{ij} + h_{ij}\right) dx^i dx^j\right]. \tag{9}$$

Within the gauge invariant formalism, we express the perturbations as equations of the density contrast δ_{DE} and the velocity divergence θ_{DE}:

$$\delta'_{DE} = -(1+w_{DE})\left(\theta_{DE} - 3\,h'\right) - 3\mathcal{H}\left(c_s^2 - w_{DE}\right)\delta_{DE}, \tag{10}$$

$$\theta'_{DE} = -\mathcal{H}\,(1-3w_{DE})\,\theta_{DE} - \frac{w'_{DE}}{1+w_{DE}}\,\theta_{DE} + \frac{c_s^2}{1+w_{DE}}\,k^2\,\delta_{DE} + k^2\,(h-\sigma_{DE})\,, \tag{11}$$

where $h(\equiv h_i^i)$ is the metric perturbation [165]. It is straightforward to figure out that perturbations of a phenomenological fluid offers two extra parameters compared to a canonical scalar field, namely, the effective sound speed c_s^2 and the anisotropic shear/stress σ_{DE}. In this work, we shall always consider a perfect fluid, so $\sigma_{DE} \equiv 0$. For the effective sound speed c_s there are various possibilities. The effective sound speed c_s importance cannot be underestimated as it reveals the microphysics associated with DE. For a barotropic fluid it is equivalent to adiabatic sound speed of the fluid, $c_s \equiv c_a$. As such no free parameters are introduced. A nice example of such a scenario is the Unparticles Dark Energy (UDE) which offers a possible resolution of Hubble and LSS tension simultaneously [149–151]. Attempting to study different microphysics, we shall consider the following scenarios:

1. Allowing dark energy either to be relativistic $c_s = 1$ or be non-relativistic $c_s = 0$.
2. A perfect fluid, with the c_s as a free parameter, $0 \leq c_s \leq 1$.

3 Data sets and methodology

In our analysis, we use the following publicly available data sets:

- **Planck 2018 CMB:** We utilize the `Planck 2018` likelihood for CMB data, which consists of low-ℓ TT, low-ℓ EE, and high-ℓ TTEETE power spectra [3]. We also use the `Planck 2018` lensing likelihood [1], which has an important role in the LSS analysis of the late Universe.
- **Baryon Acoustic Oscillations (BAO) and RSD measurements:** We use measurements from SDSS DR7 Main Galaxy Sample (MGS) [9], and 6dF galaxy survey [10] measurements at $z = 0.15$, and $z = 0.106$, respectively. In addition, we include BAO and $f\sigma_8$ measurements (where f is the linear growth rate) from BOSS DR12 & 16 at $z = 0.38, 0.51, 0.68$ [11–14], QSO measurements at $z = 1.48$ [15,16], and Ly-α auto-correlation and cross-correlation with QSO at $z = 2.2334$ [17].
- **Large Scale Structure:**

[2] It is well known that non-canonical scalar fields can give you different forms of clustering since $c_s^2 \neq 1$. In the unparticles model, the collective thermal behavior of unparticles results in a DE fluid with a temperature dependent equation of state, which in turn implies different clustering properties than a fluid with a constant equation of state.

  - **DES**: Dark Energy Survey includes measurements from shear-shear, galaxy-galaxy, and galaxy-shear two-point correlation functions, referred to as "3×2 pt", measured from 26 million source galaxies in four redshift bins and 650,000 luminous red lens galaxies in five redshift bins, for the shear and galaxy correlation functions. DES 3×2 pt likelihood gives $S_8 = 0.773^{+0.026}_{-0.020}$ and $\Omega_m = 0.267^{+0.030}_{-0.017}$ assuming the ΛCDM model [5]. To avoid computational expenses, we use a Gaussian prior on S_8 which effectively summarizes the DES likelihood. We have confirmed that using the Gaussian prior and DES likelihood provide a similar constraint.
  - **Weak Lensing Measurements:** In addition to DES, we also use measurements from KiDS+VIKING-450 and Subaru Hyper Suprime-Cam (HSC) providing constraints on S_8 and Ω_m. In this case also we use Gaussian priors to include their effects. We use $S_8 = 0.737^{+0.040}_{-0.036}$ and $S_8 = 0.780^{+0.030}_{-0.033}$ for KiDS and HSC measurements respectively.

- **Supernovae Pantheon:** The Pantheon data set is a collection of the absolute magnitude of 1048 supernovae distributed in redshift interval $0.01 < z < 2.26$ [4]. Many times we will simply refer to this data set as SN.
- **H_0 from SH0ES:** We use latest local measurement of $H_0 = 73.04 \pm 1.04$ km/s/Mpc from the SH0ES team [54]. Many times we will simply refer to this data set as H_0.

We consider several combinations of datasets to assess the parameter constraints of our phenomenological fluid dark energy model. Our aim is to compare the value of H_0 and S_8 inferred considering our model compared to the baseline model, ΛCDM. In order to quantify the degree of tension between the different estimates of H_0, we adopt the following measure to evaluate the improvement of our model compared to ΛCDM. We express the tension in terms of standard deviations σ for H_0 and S_8 as [136,166]

$$\#\sigma_{H_0} = \left| \frac{H_0^M - H_0^{\rm SH0ES}}{\sqrt{\sigma^2_{H_0^M} + \sigma^2_{H_0^{\rm SH0ES}}}} \right|, \tag{12}$$

$$\#\sigma_{S_8} = \left| \frac{S_8^M - S_8^{\rm LSS}}{\sqrt{\sigma^2_{S_8^M} + \sigma^2_{S_8^{\rm LSS}}}} \right|. \tag{13}$$

Here x^M and σ_x^M are the mean value of parameter x and its variance in a given model respectively. In the case of two measurements with asymmetric error bars $X^{\sigma_{X,\rm up}}_{\sigma_{X,\rm down}}$, $Y^{\sigma_{Y,\rm up}}_{\sigma_{Y,\rm down}}$, then the tension σ between the two measurements is:

$$\sigma = \begin{cases} \frac{X-Y}{\sqrt{\sigma^2_{X,\rm down}+\sigma^2_{Y,\rm up}}} & \text{if } X > Y \\ \frac{Y-X}{\sqrt{\sigma^2_{X,\rm up}+\sigma^2_{Y,\rm down}}} & \text{if } X \le Y. \end{cases} \tag{14}$$

This formula rigorously assesses tension between measurements, assuming the possibility of a one-tail gaussian, thus accounting for directional differences and asymmetric uncertainties, ensuring a precise and strict evaluation of the discrepancy. We investigate the following combinations of datasets:

1. Planck 2018 CMB TTTEEE power spectrum data which is one of the sources of present cosmic tensions. For simplicity, we call this dataset **Planck 2018 CMB**.
2. Combination of Primary Planck 2018 TTTEEE+ lensing data with BAO, SNe, and H_0 priors. This combination will help us understand the impact of adding other non-CMB datasets on the proposed model. We represent this combination as **CBSH**.
3. To understand the large-scale structure (S_8) tension, we also consider the full LSS data including DES-Y1, HSC, and KIDS along with Primary Planck 2018 CMB including lensing power spectra, BAO, and SNe datasets with SHOES prior. We denote this combination as **CBSHDK**.[3]
4. Finally, we remove the H_0 while using all other datasets used previously and refer to it as **CBSDK**.

The rationale for the different combinations is to see the effect of each data set on the inferred parameters, and allow for amelioration of the tension. For example, if **CBSH** prefers a lower value of S_8, closer to the WL values, and with significant $\Delta\chi^2$ improvement, then the tension is ameliorated compared to ΛCDM. The models we consider are the ΛCDM as baseline model, and extensions according to various possible PFDE. ΛCDM model has the usual 6 free independent parameters: The Baryon $\Omega_b h^2$, and Cold Dark Matter $\Omega_c h^2$ relative energy densities, the Hubble parameter H_0 or the angular scale θ_s, the amplitude A_s and tilt n_s of the primordial power spectrum, and τ_{reio} quantifying optical depth to reionization. The PFDE model offers several extra parameters namely: scale factor a_t at which dark energy eos switches sign, n the sharpness of transition which in turn affects the adiabatic sound speed c_a^2 as shown in Fig. 4, and finally the effective sound speed of perturbations c_s^2. The analysis pre-

[3] When analyzing all LSS experiments with Gaussian prior on S_8 for each data, there exists a possibility of double counting the LSS information and biasing the results as pointed out in [167]. To circumvent this issue, we have performed MCMC analysis using only a single prior on S_8. These results are tabulated in Appendices A to C. We thank Gen Ye for pointing out this issue.

sented in this paper assumes the models with parameters a_t, n and different values of c_s^2 as:

- **Canonical Emergent Dark Energy:** To begin with, we examine the specific case of setting $c_s^2 = 1$. These models fall into the category of "Canonical Emergent Dark Energy," which can be realized by employing a canonical scalar field with a suitable potential. By assigning this designation, we distinguish them as a distinct subclass within the broader framework of emergent dark energy models, [168–175].
- **Clustering Emergent Dark Energy:** Next, we assign a value of c_s^2 to zero. Under this circumstance, perturbations in DE exhibit a non-relativistic behavior and cluster akin to dark matter. Numerous investigations have focused on understanding the evolution of these perturbations and the process of structure formation in the context of clustering dark energy, [176–181].
- **Non-Canonical Emergent Dark Energy:** Moreover, we extend the parameter c_s^2 to span the range from 0 to 1. This class of models, known as non-canonical emergent dark energy models, arises from nonstandard scalar field models. In these models, the properties of dark energy are described by considering alternative formulations of scalar fields, leading to emergent behavior that deviates from canonical expectations, [182–187].

We sample the posterior distributions of the parameters describing the aforementioned models by using the Markov Chain Monte Carlo (MCMC) method. The chains are produced using the cosmological MCMC sampler `Cobaya` [188] in conjunction with modified publicly available Einstein–Boltzmann code `CAMB` [189]. The convergence of chains are guaranteed by the Gelman–Rubin parameter [190] with $R - 1 < 0.03$. We constrain the standard cosmological parameters for all cosmologies with uniform priors – the baryon matter density $\Omega_b h^2 \in [0.005, 0.1]$, the cold dark matter density $\Omega_c h^2 \in [0.001, 0.99]$, the amplitude of primordial curvature spectrum amplitude $\ln(10^{10} A_s) \in [1.6, 3.9]$ evaluated at suitable pivot scale, $k = 0.05\,\mathrm{Mpc}^{-1}$ along with its tilt $n_s \in [0.8, 1.2]$, the reionization optical depth $\tau_{reio} \in [0.01, 0.8]$ and the present value of Hubble parameter $H_0 \in [20, 100]$. We use the standard three neutrino description with one massive with mass, $m_\nu = 0.06$ eV, and two massless neutrinos. The posterior distributions are in the Supplementary Material. We work with uniform prior for a_t, n and c_s^2 with prior edges given by [0.01, 0.1], [1, 6] and [0, 1] respectively.

4 Results

In the following, we discuss the results obtained using the methods and datasets described in the previous section. This section covers the impact of emergent dark energy cosmologies on H_0 and S_8 tensions. We present 68% CL parameter inferences for ΛCDM in Table 1. We will compare the results of different models to the ΛCDM parameter constraints.

4.1 Canonical emergent dark energy cosmology

We begin our exploration by delving into the canonical emergent dark model with $c_s^2 = 1$, laying the foundation for our subsequent analysis. In order to deduce the constraints on the model parameters, we employ various combinations of data sets as outlined in Sect. 3. The resulting parameter constraints at 68% confidence level (CL) are presented in Table 2.

Considering Planck 2018 CMB data, we observe a slight increase in the derived value of $H_0 = 68.27 \pm 0.75$ for the canonical emergent dark energy models, compared to the value of $H_0 = 67.30 \pm 0.65$ for ΛCDM. This increase is consistent across other combinations of data sets, resulting in a range of H_0 values spanning from 68.3 to 69.03 km/s/Mpc in all the considered analyses. Consequently, the discrepancy known as the Hubble tension diminishes to a range of $\sim 3\sigma$ confidence level.

Table 1 The mean $\pm 1\sigma$ constraints on the cosmological parameters inferred from the various datasets for the ΛCDM model

The mean $\pm 1\sigma$ constraints for ΛCDM model				
Parameter	Planck 2018 CMB	CBSH	CBSHDK	CBSDK
H_0	67.30 ± 0.65	$68.09^{+0.63}_{-0.41}$	$68.13^{+0.86}_{-0.32}$	$68.16^{+0.37}_{-0.32}$
σ_8	0.8117 ± 0.0079	0.8102 ± 0.0063	0.8055 ± 0.0058	0.8056 ± 0.0060
S_8	0.833 ± 0.017	$0.818^{+0.010}_{-0.015}$	$0.8119^{+0.0082}_{-0.017}$	0.8114 ± 0.0094
Ω_m	0.3162 ± 0.0089	$0.3056^{+0.0051}_{-0.0083}$	$0.3048^{+0.0039}_{-0.011}$	$0.3043^{+0.0040}_{-0.0048}$
$\#\sigma_{H_0}$	4.68	4.07	3.63	4.42
$\#\sigma_{S_8}$	2.28	1.89	1.72	1.81
Total χ^2	2764.17	3854.028	3859.8118	3846.0773
$\Delta\chi^2$	–	–	–	–

Table 2 The mean $\pm 1\sigma$ constraints on the cosmological parameters inferred from the various datasets for canonical emergent dark energy model ($c_s^2 = 1$) model

The mean $\pm 1\sigma$ constraints for canonical emergent dark energy model ($c_s^2 = 1$)				
Parameter	Planck 2018 CMB	CBSH	CBSHDK	CBSDK
H_0	68.27 ± 0.75	$68.94^{+0.43}_{-0.62}$	69.03 ± 0.50	68.72 ± 0.39
σ_8	0.8112 ± 0.0087	$0.8134^{+0.0067}_{-0.0078}$	0.8078 ± 0.0066	0.8070 ± 0.0062
S_8	0.820 ± 0.016	0.812 ± 0.011	0.8043 ± 0.0092	0.8081 ± 0.0087
Ω_m	0.3068 ± 0.0092	$0.2993^{+0.0067}_{-0.0054}$	0.2974 ± 0.0054	0.3009 ± 0.0046
$10^2\, a_t$	$3.400^{+0.071}_{-0.023}$	$3.50^{+0.11}_{-0.32}$	$3.425^{+0.080}_{-0.26}$	$3.368^{+0.056}_{-0.20}$
c_s^2	1	1	1	1
n	> 2.86	> 3.08	> 3.02	> 2.88
$c_{a_0}^2$	0.23 ± 0.46	0.28 ± 0.41	0.27 ± 0.43	0.24 ± 0.44
$\#\sigma_{H_0}$	3.72	3.64	3.47	3.88
$\#\sigma_{S_8}$	1.92	1.80	1.63	1.73
Total χ^2	2766.1977	3852.5094	3857.234	3846.1532
$\Delta\chi^2$	2.0277	-1.5186	-2.5778	0.0759

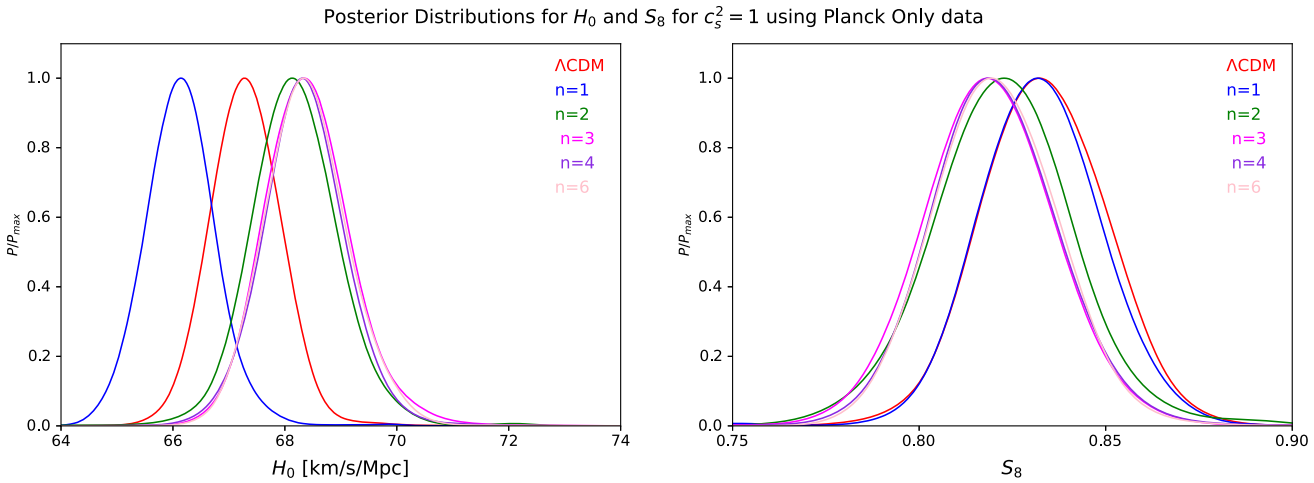

Fig. 5 Normalized posterior distributions for H_0 (in km/s/Mpc) and S_8 in left and right panels respectively for different choices of n for Canonical Emergent Dark Energy model with $c_s^2 = 1$, using Primary Planck 2018 CMB data. We also show the constraints for the ΛCDM model for comparison

Moreover, we find a marginal decrease in the inferred values of S_8 within this framework. For instance, when considering only the Planck data, the inferred value of S_8 is 0.82 ± 0.016, whereas other data sets yield similar values ranging from 0.804 to 0.82. This decrease in S_8 can be attributed to the reduction in matter energy density, which exhibits a decrease of approximately 1%.

Moving forward, we shift our focus to the inference of the model parameters a_t and either n or $c_{a_0}^2$. In order to derive the functional dependence of $c_{a_0}^2$ on other parameters, one can simply evaluate the Eq. (8) at $z = 0$. Our analysis reveals that the 68% CL evidence points to $10^2\, a_t = 3.4^{+0.071}_{-0.023}$. Additionally, we constrain the adiabatic sound speed of dark energy at the present time, denoted as $c_{a_0}^2$. The analysis indicates positive adiabatic sound speed with $c_{a_0}^2 = 0.27^{+0.60}_{-0.36}$ at the 68% CL when considering only the Planck data. Furthermore, we establish a lower bound on the parameter n, demonstrating that cosmological data favors the canonical emergent dark energy model while excluding the presence of ghost or gradient stability. Our findings indicate $n > 2.88$, and Fig. 4 confirms that for $n > 2$, the adiabatic sound speed lies within the range of [0, 1].

We evaluate the goodness-of-fit for various combinations in the canonical emergent dark energy scenario and compare them with ΛCDM. We observe that the fit to the Planck-only data yields a larger value of $\Delta\chi^2 = 2.0277$, indicating a less

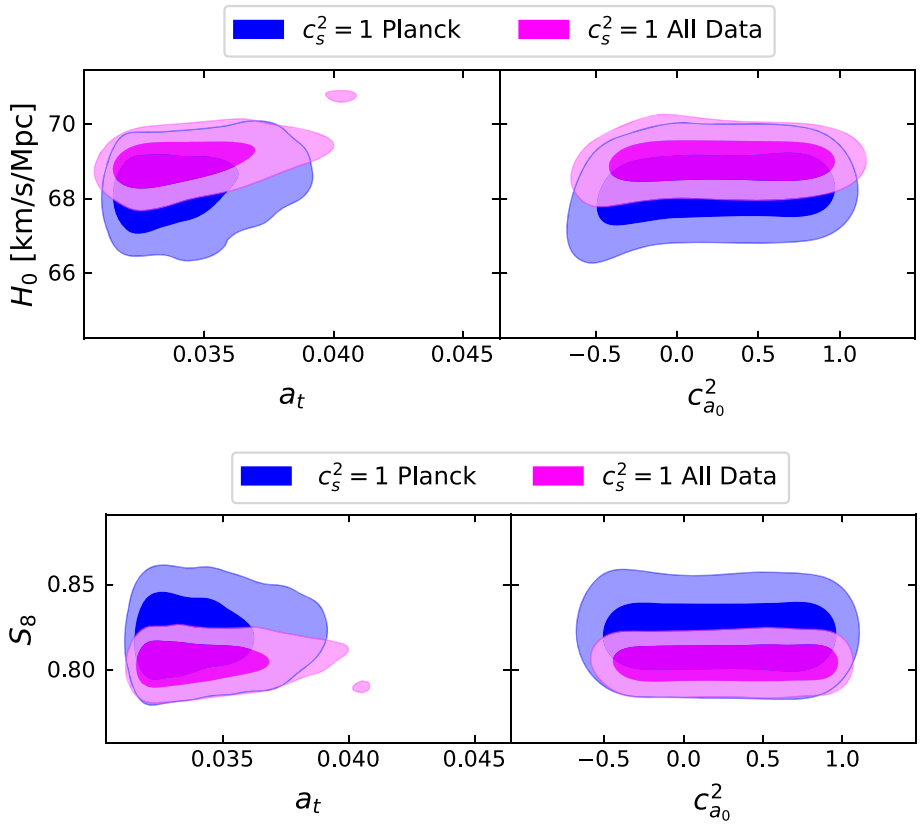

Fig. 6 2-Dimensional marginalized posterior distributions for model parameters a_t and $c^2_{a_0}$ (and hence n) with H_0 and S_8 in upper and lower panels for canonical emergent dark energy model. The blue and magenta correspond to Primary Planck 2018 CMB data and All data described in Sect. 3

favorable fit. However, as we combine the Planck data with several other data sets, we witness an improvement reaching approximately $\Delta\chi^2 = -2.6$ in our analysis.

We also study the impact of different values of n which in turn means that $c^2_{a_0}$ is fixed. We fixed the values of n spanning from 1 to 6. The resulting constraints for different combination are shown in Appendix A (Tables 5, 6, 7, 8, 9). The normalized 1-dimensional posterior distributions for H_0 in units of km/s/Mpc and S_8 for different values of n in this scenario using the Primary Planck 2018 CMB data in Fig. 5. We notice an increase in the inferred value of H_0 and a decrease in the inferred value of S_8 except for $n = 1$, which is prone to ghost instability. This trend is present in other data-sets combinations as well.

Finally, we close this subsection by discussing the correlation of model parameters, a_t and $c^2_{a_0}$ or n, with H_0 and S_8 considering the various datasets. Upper and lower panels of Fig. 6 show the 2-dimensional contours of $H_0 - (a_t, c^2_{a_0})$ and $S_8 - (a_t, c^2_{a_0})$ respectively. The blue contours are using only Planck data, while the magenta contours take into account all data. In all cases we considered $c_s^2 = 1$. It is evident from the Fig. 6 that in canonical emergent dark energy scenarios H_0 and S_8 are rather insensitive to n, and that a_t is constrained. Comparing to ΛCDM the model infers a higher value for H_0 and a lower one for S_8 (Fig. 5).

4.2 Clustering emergent dark energy cosmology

Let us consider the Clustering Emergent Dark Energy case, that corresponds to $c_s = 0$ on various data sets. The parameter constraints at the 68% confidence level (CL) are presented in Table 3, alongside the best-fit χ^2 and $\Delta\chi^2$ compared to ΛCDM.

We observe an increase in the derived values of H_0 and S_8 compared to the Primary Planck 2018 CMB data analysis. Hence, while there is a marginal improvement in the H_0 value, the S_8 value worsens in comparison to the canonical emergent dark energy cosmologies using Primary Planck 2018 CMB data. The 1-D posterior distributions for H_0 and S_8 are shown in Fig. 7. Because DE can cluster in this model, we find an increment in $\sigma_8 = 0.838^{+0.033}_{-0.0057}$. This increase in σ_8 is solely responsible for the worsening of the S_8 tension.

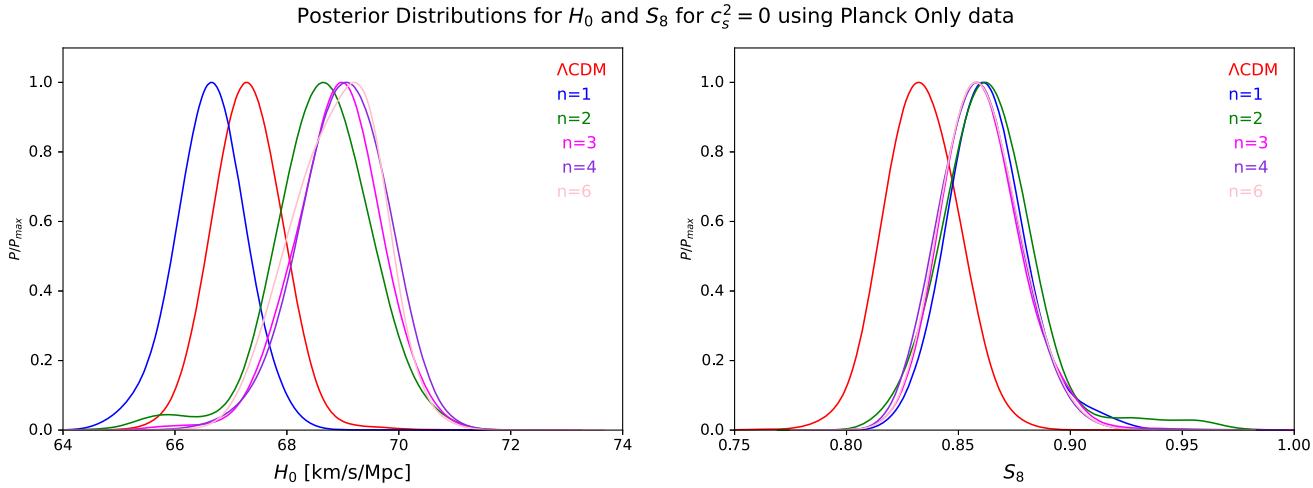

Fig. 7 Normalized posterior distributions for H_0 (in km/s/Mpc) and S_8 in left and right panels respectively for different choices of n for the Clustering Emergent Dark Energy model with $c_s^2 = 0$ using Primary Planck 2018 CMB data. We also show the constraints for the ΛCDM model for comparison

Table 3 The mean $\pm 1\sigma$ constraints on the cosmological parameters inferred from the various datasets for clustering emergent dark energy ($c_s^2 = 0$) model

The mean $\pm 1\sigma$ constraints for clustering emergent dark energy ($c_s^2 = 0$) model				
Parameter	Planck 2018 CMB	CBSH	CBSHDK	CBSDK
H_0	$68.7^{+1.0}_{-0.78}$	$68.61^{+0.67}_{-0.41}$	$69.00^{+0.53}_{-0.34}$	68.96 ± 0.40
σ_8	$0.838^{+0.023}_{-0.0057}$	$0.846^{+0.012}_{-0.0093}$	$0.814^{+0.014}_{-0.016}$	$0.8422^{+0.0052}_{-0.0070}$
S_8	$0.837^{+0.030}_{-0.011}$	$0.846^{+0.014}_{-0.012}$	$0.808^{+0.013}_{-0.018}$	$0.8369^{+0.0084}_{-0.096}$
Ω_m	$0.2993^{+0.0093}_{-0.011}$	$0.3001^{+0.0049}_{-0.0068}$	$0.2958^{+0.0042}_{-0.0057}$	$0.2963^{+0.0044}_{-0.0051}$
$10^2\, a_t$	$3.288^{+0.033}_{-0.12}$	$3.255^{+0.022}_{-0.092}$	$3.239^{+0.017}_{-0.077}$	$3.400^{+0.069}_{-0.23}$
c_s^2	0	0	0	0
n	< 3.17	< 3.14	$3.67^{+0.47}_{-0.12}$	> 3.07
$c_{a_0}^2$	$-0.14^{+0.39}_{-0.50}$	-0.16 ± 0.30	$0.225^{+0.16}_{+0.039}$	$0.28^{+0.64}_{-0.32}$
$\#\sigma_{H_0}$	3.00	3.58	3.46	3.66
$\#\sigma_{S_8}$	2.41	2.61	1.61	0.96
Total χ^2	2767.1379	3852.2095	3859.1056	3857.8257
$\Delta\chi^2$	2.9679	−1.8185	−0.7062	+11.74

The model parameters $10^2\, a_t$ and n (or $c_{a_0}^2$) are reported as $3.288^{+0.033}_{-0.12}$ and < 3.17 ($-0.14^{+0.38}_{-0.50}$), respectively.

Next, we examine the consequences of considering other data sets within this scenario. The present values of the Hubble parameter H_0 and the amplitude of matter fluctuations S_8 follow the same trends across different data sets and their combinations. The inferred values of H_0 and S_8 lie within the ranges of [68−69] km/s/Mpc, and [0.808−0.843] respectively, for the other combinations. The predictions of the model, represented by a_t and n (or the derived parameter $c_{a_0}^2$), reveal a transition redshift a_t of approximately 0.034. The possible correlations between additional model parameters and H_0 and S_8 are illustrated in Fig. 8. The 68% constraint for different n are shown in Appendix B, Tables 10, 11, 12, 13, 14.

Finally, we conclude the discussion on clustering in emergent dark energy by commenting on the χ^2 and $\Delta\chi^2$. In this scenario, we observe a worse fit to the data compared to our baseline model ΛCDM and the canonical emergent dark energy case. As mentioned earlier, while it is possible to alleviate the Hubble tension in this scenario, the tension related to large-scale structure becomes more pronounced.

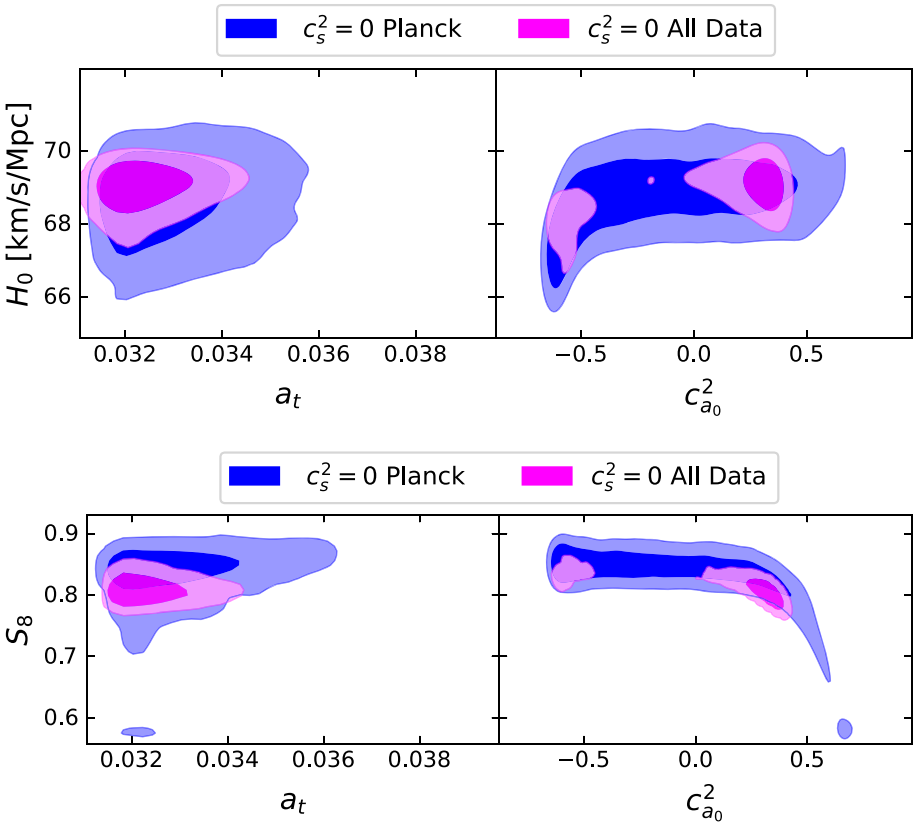

Fig. 8 2-Dimensional marginalized posterior distributions for model parameters a_t and $c^2_{a_0}$ (and hence n) with H_0 and S_8 in upper and lower panels for clustering emergent dark energy model. These plots show the correlation between model parameters with H_0 and S_8. The blue and magenta correspond to Primary Planck 2018 CMB data and All data sets described in Sect. 3

Table 4 The mean $\pm 1\sigma$ constraints on the cosmological parameters inferred from the various datasets for non-canonical emergent dark energy (open c_s^2) model

The mean $\pm 1\sigma$ constraints for non-canonical emergent dark energy (open c_s^2) model				
Parameter	Planck 2018 CMB	CBSH	CBSHDK	CBSDK
H_0	$68.30^{+0.84}_{-0.72}$	$68.82^{+0.45}_{-0.39}$	$69.00^{+0.48}_{-0.32}$	68.73 ± 0.41
σ_8	0.8133 ± 0.0093	$0.8147^{+0.0066}_{-0.0080}$	$0.8092^{+0.0059}_{-0.0070}$	$0.8086^{+0.0060}_{-0.0069}$
S_8	0.822 ± 0.017	$0.8155^{+0.0091}_{-0.011}$	$0.8063^{+0.0079}_{-0.010}$	0.8098 ± 0.0093
Ω_m	$0.3066^{+0.0089}_{-0.010}$	$0.3006^{+0.0045}_{-0.0052}$	$0.2979^{+0.0036}_{-0.0055}$	0.3009 ± 0.0046
$10^2\, a_t$	$3.374^{+0.056}_{-0.21}$	$3.423^{+0.082}_{-0.25}$	$3.381^{+0.061}_{-0.21}$	$3.338^{+0.045}_{-0.17}$
c_s^2	$0.65^{+0.26}_{-0.17}$	$0.66^{+0.22}_{-0.19}$	$0.68^{+0.26}_{-0.14}$	> 0.597
n	3.45 ± 1.45	$3.8^{+1.8}_{-1.1}$	> 2.95	> 3.06
$c^2_{a_0}$	0.15 ± 0.48	$0.26^{+0.62}_{-0.43}$	0.24 ± 0.44	0.27 ± 0.46
$\#\sigma_{H_0}$	3.54	3.72	3.52	3.85
$\#\sigma_{S_8}$	1.95	1.89	1.68	1.77
Total χ^2	2765.8647	3851.7445	3856.9329	3846.0359
$\Delta\chi^2$	1.6947	−2.2835	−2.8789	−0.0414

4.3 Non-canonical emergent dark energy

Finally, we investigate the implications of non-canonical emergent dark energy by allowing the effective sound speed (c_s^2) to vary between 0 to 1, along with other model parameters. We present the parameter constraints for this case in Table 4. Similar to previous cases, we find an increase in the value of H_0 and a marginal decrease in S_8. Ana-

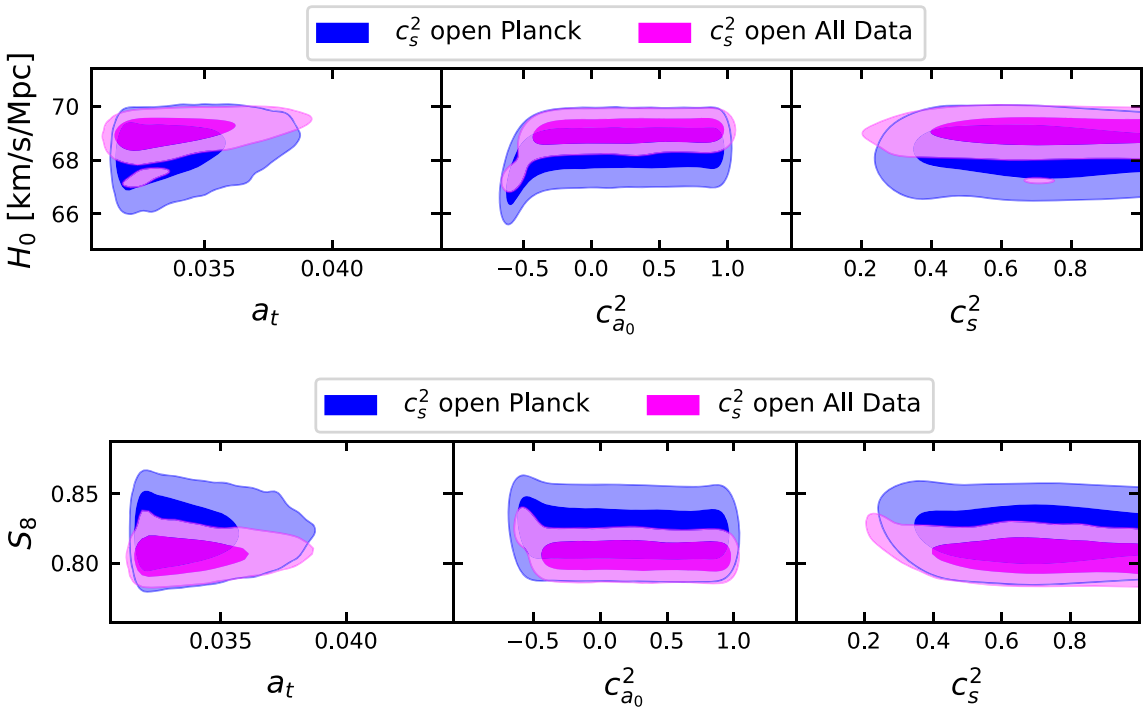

Fig. 9 2-Dimensional marginalized posterior distributions for model parameters a_t and c_{a0}^2 (and hence n) with H_0 and S_8 in upper and lower panels for non-canonical emergent dark energy model. These plots show the correlation between model parameters with H_0 and S_8. The blue and magenta correspond to Primary Planck 2018 CMB data and all data sets described in Sect. 3

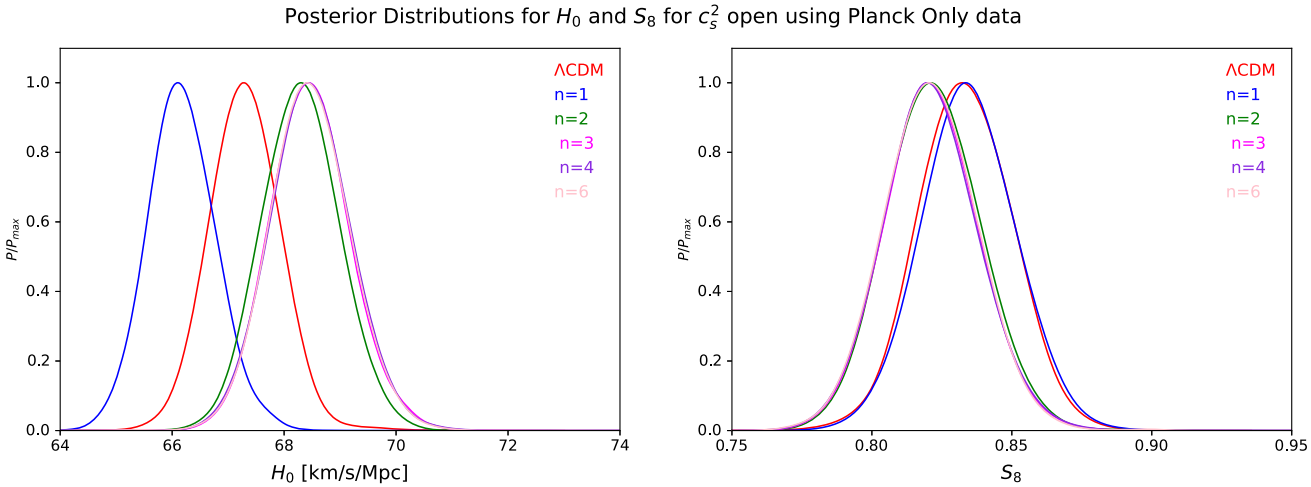

Fig. 10 Normalized posterior distributions for H_0 (in km/s/Mpc) and S_8 in left and right panels respectively for different choices of n for Emergent Dark Energy model keeping c_s^2 open, and using Primary Planck 2018 CMB data. We also show the ΛCDM results for comparison

lyzing the Primary Planck 2018 Cosmic Microwave Background (CMB) data, we infer $H_0 = 68.30^{+0.51}_{-0.72}$ km/s/Mpc and $S_8 = 0.822 \pm 0.017$. The amplitude of matter fluctuations σ_8 and matter density Ω_m are constrained to be 0.8133 ± 0.0093 and $0.3066^{+0.0089}_{-0.010}$ respectively. The tension metrics for H_0 and S_8 show an improvement of approximately 1σ and 0.5σ respectively. Moving to other data sets, the improvement in H_0 and S_8 remains consistent, resulting in $H_0 \approx 68.8$ km/s/Mpc and $S_8 \approx 0.81$.

In all cases considered, we find the transition scale factor to be approximately $a_t = 0.034$, regardless of the data set used. The steepness parameter n is constrained to ensure that

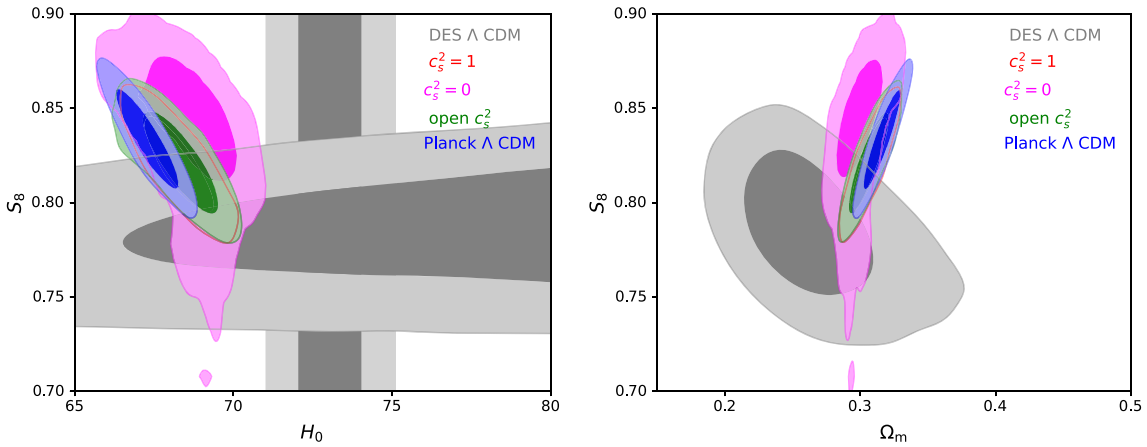

Fig. 11 Left panel: comparison of H_0 and S_8 for the ΛCDM and emergent dark energy with different c_s^2. The horizontal and vertical axis represent the H_0 in units of km/s/Mpc and S_8 respectively. We denote as ΛCDM as blue, $c_s^2 = 1$ as red, $c_s^2 = 0$ as magenta and c_s^2 open as green. The dark and light shaded regions correspond to the 68% and 95% confidence level (CL) respectively. Right panel: comparison of Ω_m and S_8 as horizontal and vertical axis respectively with similar color codes. In both plots the local SH0ES and DES measurements are expressed in gray

c_a^2 remains free from gradient/ghost instabilities and subluminal throughout the evolution. Using the Primary Planck 2018 CMB data in combination with Baryon Acoustic Oscillations (BAO), Supernovae (SNe), and for the SH0ES measurement, we find that $n = 3.8^{+1.8}_{-1.1}$ and, consequently, $c_{a_0}^2 = 0.26^{+0.62}_{-0.43}$. The effective sound speed of perturbations, c_s^2, is determined to be 0.27 ± 0.46 for the same data set. The correlation between the model parameters (a_t, $c_{a_0}^2$, and c_s^2) with H_0 and S_8 is depicted in Fig. 9, demonstrating that H_0 and S_8 are insensitive to the values of n, $c_{a_0}^2$, and c_s^2. Except for Planck 2018 alone, the non-canonical emergent dark energy model provides a better fit to the data, regardless of the data sets considered. The difference in χ^2 compared to the ΛCDM model ranges from -0.04 to -2.88.

Next, we explore the impact of different values of n in this scenario. Figure 10 displays the 1-dimensional normalized probability distribution for H_0 and S_8 for n ranging from 1 to 6, using the Primary Planck 2018 CMB data. For $n = 1$, the model is disfavored as it yields $\Delta\chi^2 \in [2, 13]$ and predicts a lower H_0 and slightly higher value of S_8. As observed in the case of open n, for $n \in [3, 6]$, we find an improvement in both H_0 and S_8 simultaneously, providing a better fit compared to the ΛCDM model and cases with $c_s^2 = 1$ or 0. The 68% constraint for different n are shown in Appendix C Tables 15, 16, 17, 18, 19.

We compare all three models analyzed in this paper with ΛCDM in Fig. 11. The Primary Planck 2018 CMB constraints for ΛCDM, and Emergent DE model with $c_s^2 = 1$, $c_s^2 = 0$ and c_s^2 open are denoted as blue, red, magenta, and green respectively. The shaded dark and light regions correspond to the 68% and 95% confidence levels, respectively. We also compare the results with the latest local SH0ES and DES-Y1 measurements. It is clear from both the left and right panels of Fig. 11 that canonical and non-canonical dark energy models offer a marginal increase in values of H_0 and a marginal decrease in S_8.

5 Conclusions

We have studied the emergent dark energy model by considering the phenomenological fluid approach. This approach offers to probe the arbitrary sound speed of dark energy perturbations. The emergent dark energy behaves like a cosmological constant (Λ) at late times and asymptotes to a radiation fluid at early times. As such, it incorporates a tracking mechanism and allows for a rather sudden transition in the DE eos. We employed a phenomenological fluid with 2 parameters to mimic this feature. These two parameters are the scale factor, at which the equation of state of the phenomenological fluid crosses 0, a_t, and the steepness parameter n. In addition to these parameters, we also have an arbitrary sound speed of dark energy perturbations c_s^2 taking values within the range of 0 to 1. In this paper, we considered the three different case of $c_s^2 = 1$, $c_s^2 = 0$ and c_s^2 open which we assigned them as canonical, clustering, and non-canonical emergent dark energy models. The consideration of each case is capable of explaining the current accelerated expansion of the Universe, and avoids the coincidence problem due to the inherent tracking mechanism. We showed the impact of a_t and n on the evolution of the background and perturbations. The background behavior is illustrated in Figs. 1 and 2. We found that there exists a threshold value of a_t in order to get an era of

matter domination, as required for structure formation. The adiabatic sound speed c_a^2 which depends both on a_t and n is shown in Fig. 4. It is worth mentioning that c_a^2 has strong dependence on n. The left panel of Fig. 4 clearly shows that for $n \geq 3$, c_a^2 lies with in range of [0, 1] further constraining the parameter space. Hence, $n \geq 3$ is preferred on theoretical grounds.

We then analyzed the parameter constraints using the different cosmic data-sets. The aim of the exercise was to check the ability of alleviating the cosmological tensions (H_0 and S_8) in the emergent dark energy scenario. We considered the various data-sets to assess the impact of model in reducing the cosmic tensions. We noticed an overall improvement of both tensions for all models considered. Out of all the models considered in our analysis, we found that keeping c_s^2 open i.e. non-canonical emergent dark energy provides the best improvement with respect to ΛCDM. The canonical model also reduces both cosmic tensions while clustering (non-relativistic) model reduces the Hubble constant tension and worsens the LSS tension. During our analysis, we chose a wide prior on $n \in [1, 6]$, being agnostic about the fact that $n \leq 3$ makes the evolution problematic and let the data decide to constrain the value of n. Interestingly, we found that most of the data-sets constrain the value of n respecting the theoretical arguments and prefer $n \geq 3$.

The reduction in the Hubble and LSS tension is rather mild and not very significant statistically. This is probably a reflection of the fact that H_0 and S_8 seem rather insensitive to a_t and n. The main difference in the current analysis compared to the emergent unparticles DE model (UDE) [149] is that here the adiabatic speed of sound c_a^2 and the effective sound speed c_s^2 were different, while in the UDE they were equal. Given that in the UDE we got a much more significant reduction of the tensions in a statistically significant way, highlights the important role the adiabatic and effective sound speeds play in inferring the cosmological parameters. Given the insensitivity to n it seems that fixing n and c_s^2 and leaving only a_t as a free parameter can be competitive with the wCDM model, and can be constrained significantly with current and future data. The most intriguing result in our opinion is the fact that the transition redshift is highly limited with $29 < 1 + z < 30$. As a result one can think of ways to try and detect such a transition.

Acknowledgements We acknowledge the Ariel HPC Center at Ariel University for providing computing resources that have contributed to the research results reports reported within this paper.

Data Availability Statement This manuscript has data included as electronic supplementary material. The online version of this article contains supplementary material, which is available to authorized users.

Funded by SCOAP[3].

Appendices

In the following appendices Appendices A to C, we provide the parameter constraints for different dark energy models. These models are special cases of canonical, clustering and non-canonical dark energy models for fixed values of n. We consider the same combination of data-sets as mentioned in Sect. 3. The various tables summarize the parameter constraints at 1 σ CL for different values of n from 1 to 6.

Appendix A. Canonical emergent dark energy

See Table 5.

Table 5 The mean $\pm 1\sigma$ (best-fit) constraints on the cosmological parameters inferred from the *Planck* 2018 CMB data (including TTEETE) for Canonical Emergent DE scenario with different values of n varying from 1 to 6

The mean $\pm 1\sigma$ constraints from Planck 2018 CMB for $c_s^2 = 1$ for different n					
Parameter	$n = 1$	$n = 2$	$n = 3$	$n = 4$	$n = 6$
H_0	66.15 ± 0.68	68.18 ± 0.87	$68.42^{+0.68}_{-0.83}$	68.35 ± 0.75	$68.39^{+0.68}_{-0.79}$
σ_8	$0.7973^{+0.0073}_{-0.0084}$	$0.8122^{+0.0081}_{-0.0097}$	0.8115 ± 0.0096	0.8120 ± 0.0094	$0.8128^{+0.0074}_{-0.0090}$
S_8	0.832 ± 0.017	0.823 ± 0.021	0.819 ± 0.018	0.820 ± 0.018	0.821 ± 0.017
Ω_m	0.3270 ± 0.0095	0.308 ± 0.011	0.3055 ± 0.0098	0.3063 ± 0.0094	0.3059 ± 0.0094
$10^2\, a_t$	$3.470^{+0.075}_{-0.31}$	$3.429^{+0.056}_{-0.27}$	$3.421^{+0.057}_{-0.26}$	$3.390^{+0.068}_{-0.23}$	$3.417^{+0.051}_{-0.25}$
Total χ^2	2766.0376	2765.8973	2765.8248	2766.1938	2765.7482
$\Delta\chi^2$	1.8676	1.7273	1.6548	2.0238	1.5782

A.1. Planck + Lensing + BAO + SN + H_0

See Table 6

A.2. Planck + Lensing + BAO + SN + H_0 + DES-Y1

See Table 7.

A.3. Planck + Lensing + BAO + SN + H_0 + DES-Y1 + HSC + KIDS

See Table 8.

Table 6 The mean $\pm 1\sigma$(best-fit) constraints on the cosmological parameters inferred from the *Planck* 2018 CMB data (including TTEETE + lensing), BAO, SNe and SH0ES data for Canonical Emergent DE scenario for different values of n

The mean $\pm 1\sigma$ constraints from Planck 2018 + Lensing + BAO + SN + H_0					
Parameter	$n = 1$	$n = 2$	$n = 3$	$n = 4$	$n = 6$
H_0	$67.33^{+0.67}_{-0.51}$	$68.88^{+0.62}_{-0.89}$	$68.85^{+0.48}_{-0.59}$	$68.96^{+0.49}_{-0.80}$	$68.90^{+0.50}_{-0.60}$
σ_8	$0.7985^{+0.0065}_{-0.0081}$	$0.8139^{+0.0065}_{-0.0088}$	$0.8141^{+0.0062}_{-0.0082}$	$0.8141^{+0.0063}_{-0.0086}$	$0.8137^{+0.0060}_{-0.0081}$
S_8	$0.812^{+0.011}_{-0.015}$	0.814 ± 0.016	$0.8149^{+0.0096}_{-0.012}$	0.813 ± 0.014	$0.814^{+0.010}_{-0.011}$
Ω_m	$0.3105^{+0.0062}_{-0.0092}$	$0.3000^{+0.0091}_{-0.0081}$	0.3006 ± 0.0082	$0.2995^{+0.0084}_{-0.0065}$	0.3000 ± 0.0075
$10^2\, a_t$	$3.58^{+0.10}_{-0.41}$	$3.54^{+0.11}_{-0.37}$	$3.500^{+0.089}_{-0.32}$	$3.514^{+0.091}_{-0.35}$	$3.496^{+0.090}_{-0.32}$
Total χ^2	3869.1753	3852.9131	3851.876	3852.3776	3852.1676
$\Delta\chi^2$	15.5434	− 1.0037	− 1.2103	− 0.9626	− 1.2265

Table 7 The mean $\pm 1\sigma$(best-fit) constraints on the cosmological parameters inferred from the *Planck* 2018 CMB data (including TTEETE + lensing), BAO, SNe, SH0ES and DES-Y1 data for Canonical Emergent DE scenario for different values of n

Constraints from Planck 2018 + Lensing + BAO + SN + H_0 + DES for Canonical Emergent DE						
Parameter	$n = 1$	$n = 2$	$n = 3$	$n = 4$	$n = 6$	n open
H_0	67.59 ± 0.64	$68.75^{+0.51}_{-0.41}$	$68.82^{+0.45}_{-0.40}$	$69.01^{+0.44}_{-0.56}$	$68.99^{+0.45}_{-0.51}$	$68.93^{+0.53}_{-0.41}$
σ_8	$0.7972^{+0.0064}_{-0.0081}$	$0.8110^{+0.0062}_{-0.0074}$	$0.8117^{+0.0059}_{-0.0073}$	$0.8126^{+0.0061}_{-0.0079}$	$0.8123^{+0.0063}_{-0.0075}$	$0.8107^{+0.0065}_{-0.0075}$
S_8	$0.8063^{+0.0095}_{-0.012}$	$0.8121^{+0.0082}_{-0.012}$	$0.8123^{+0.0087}_{-0.011}$	0.810 ± 0.011	0.810 ± 0.011	$0.8092^{+0.0089}_{-0.010}$
Ω_m	0.3070 ± 0.0081	$0.3009^{+0.0046}_{-0.0063}$	$0.3005^{+0.0043}_{-0.0057}$	$0.2984^{+0.0061}_{-0.0053}$	0.2986 ± 0.0066	$0.2990^{+0.0046}_{-0.0062}$
$10^2\, a_t$	$3.58^{+0.11}_{-0.41}$	$3.456^{+0.096}_{-0.28}$	$3.441^{+0.096}_{-0.27}$	$3.47^{+0.10}_{-0.29}$	$3.47^{+0.10}_{-0.30}$	$3.462^{+0.094}_{-0.29}$
n	1	2	3	4	6	> 3.05
Total χ^2	3869.5714	3853.0243	3852.8177	3853.0654	3852.8015	3854.1713
$\Delta\chi^2$	13.843	− 2.7041	− 2.9107	− 2.663	− 2.9269	− 1.55

Table 8 The mean $\pm 1\sigma$ constraints on the cosmological parameters inferred from the *Planck* 2018 CMB data (including TTEETE + lensing), BAO, SNe, SH0ES, DES-Y1 and weak-lensing data for Canonical Emergent DE scenario for different values of n

Constraints from Planck 2018 + Lensing + BAO + SN + H_0 + DES + HSC + KIDS for Canonical Emergent DE					
Parameter	$n = 1$	$n = 2$	$n = 3$	$n = 4$	$n = 6$
H_0	$67.61^{+0.46}_{-0.40}$	69.01 ± 0.68	$69.16^{+0.42}_{-0.57}$	$69.16^{+0.39}_{-0.44}$	$68.99^{+0.49}_{-0.44}$
σ_8	$0.7933^{+0.0055}_{-0.0074}$	$0.8076^{+0.0055}_{-0.0069}$	$0.8088^{+0.0055}_{-0.0080}$	$0.8077^{+0.0058}_{-0.0069}$	0.8083 ± 0.0071
S_8	$0.8016^{+0.0082}_{-0.011}$	$0.8041^{+0.0088}_{-0.0099}$	0.804 ± 0.011	0.803 ± 0.010	$0.8057^{+0.0079}_{-0.0097}$
Ω_m	$0.3064^{+0.0046}_{-0.0064}$	$0.2975^{+0.0049}_{-0.0057}$	0.2965 ± 0.0078	0.2962 ± 0.0049	$0.2981^{+0.0044}_{-0.0057}$
$10^2\, a_t$	$3.529^{+0.089}_{-0.36}$	$3.434^{+0.077}_{-0.26}$	$3.474^{+0.057}_{-0.30}$	$3.441^{+0.091}_{-0.27}$	$3.405^{+0.077}_{-0.23}$
Total χ^2	3873.4982	3857.2683	3857.9786	3856.8311	3857.0445
$\Delta\chi^2$	13.6864	− 2.5435	− 1.8332	− 2.9807	− 2.7673

A.4. Planck + Lensing + BAO + SN + DES-Y1 + HSC + KIDS

See Table 9.

Appendix B. Clustering emergent dark energy

B.1. Planck TTTEEE only

See Table 10.

B.2. Planck + Lensing + BAO + SN + H_0

See Table 11.

Table 9 The mean $\pm 1\sigma$ constraints on the cosmological parameters inferred from the *Planck* 2018 CMB data (including TTEETE + lensing), BAO, SNe, DES-Y1 and weak-lensing data for Canonical Emergent DE scenario for different values of n

Constraints from Planck 2018 + Lensing + BAO + SN + DES + KIDS + HSC for Canonical Emergent DE					
Parameter	$n = 1$	$n = 2$	$n = 3$	$n = 4$	$n = 6$
H_0	$67.23^{+0.41}_{-0.32}$	$68.63^{+0.37}_{-0.33}$	$68.76^{+0.33}_{-0.39}$	68.74 ± 0.40	68.77 ± 0.39
σ_8	0.7921 ± 0.0078	0.8058 ± 0.0069	0.8078 ± 0.0075	$0.8075^{+0.0054}_{-0.0062}$	$0.8074^{+0.0056}_{-0.0064}$
S_8	$0.8068^{+0.0079}_{-0.010}$	$0.8080^{+0.0084}_{-0.0097}$	0.8087 ± 0.0094	0.8086 ± 0.0094	0.8080 ± 0.0085
Ω_m	$0.3112^{+0.0040}_{-0.0059}$	$0.3017^{+0.0036}_{-0.0049}$	$0.3006^{+0.0045}_{-0.0038}$	0.3008 ± 0.0049	0.3004 ± 0.0045
$10^2\, a_t$	$3.473^{+0.076}_{-0.31}$	$3.379^{+0.058}_{-0.21}$	$3.383^{+0.060}_{-0.22}$	$3.36^{+0.12}_{-0.20}$	$3.358^{+0.052}_{-0.19}$
Total χ^2	3853.8996	3846.3778	3846.0869	3845.8107	3846.0881
$\Delta\chi^2$	7.8223	0.3005	0.0096	− 0.2666	0.0108

Table 10 The mean $\pm 1\sigma$ constraints on the cosmological parameters inferred from the *Planck* 2018 CMB data (including TTEETE) for Clustering Emergent DE scenario for different values of n

Constraints from Planck 2018 CMB for Clustering Emergent Dark Energy					
Parameter	$n = 1$	$n = 2$	$n = 3$	$n = 4$	$n = 6$
H_0	66.63 ± 0.65	68.62 ± 0.93	$68.90^{+0.82}_{-0.73}$	$69.02^{+0.84}_{-0.74}$	$68.89^{+0.90}_{-0.72}$
σ_8	$0.8371^{+0.0080}_{-0.012}$	$0.8633^{+0.0092}_{-0.012}$	$0.8638^{+0.0089}_{-0.012}$	$0.8649^{+0.0080}_{-0.013}$	$0.8632^{+0.0086}_{-0.012}$
S_8	$0.863^{+0.016}_{-0.019}$	$0.864^{+0.018}_{-0.022}$	$0.861^{+0.016}_{-0.020}$	$0.859^{+0.017}_{-0.019}$	$0.860^{+0.016}_{-0.019}$
Ω_m	$0.3189^{+0.0086}_{-0.0099}$	$0.3009^{+0.0095}_{-0.012}$	$0.2979^{+0.0087}_{-0.011}$	$0.2964^{+0.0090}_{-0.011}$	$0.2980^{+0.0087}_{-0.012}$
$10^2\, a_t$	$3.335^{+0.051}_{-0.17}$	$3.274^{+0.029}_{-0.11}$	$3.289^{+0.052}_{-0.13}$	$3.283^{+0.032}_{-0.12}$	$3.268^{+0.039}_{-0.10}$
Total χ^2	2764.9465	2766.3194	2766.6314	2766.6984	2766.6043
$\Delta\chi^2$	0.7765	2.1494	2.4614	2.5284	2.4343

Table 11 The mean $\pm 1\sigma$ constraints on the cosmological parameters inferred from the *Planck* 2018 CMB data (including TTEETE + lensing), BAO, SNe and SH0ES for Clustering Emergent DE scenario for different values of n

Constraints from Planck 2018 + Lensing + BAO + SN + H_0 for clustering emergent dark energy					
Parameter	$n = 1$	$n = 2$	$n = 3$	$n = 4$	$n = 6$
H_0	$67.34^{+0.69}_{-0.29}$	$68.51^{+0.70}_{-0.38}$	$68.76^{+0.63}_{-0.46}$	$68.74^{+0.71}_{-0.43}$	$68.65^{+0.41}_{-0.35}$
σ_8	$0.8365^{+0.0063}_{-0.012}$	$0.8551^{+0.0059}_{-0.0091}$	$0.8540^{+0.0048}_{-0.011}$	$0.8145^{+0.0068}_{-0.010}$	$.8581^{+0.0061}_{-0.0076}$
S_8	$0.8487^{+0.0093}_{-0.019}$	$0.8578^{+0.0087}_{-0.016}$	$0.8531^{+0.0083}_{-0.017}$	$0.814^{+0.011}_{-0.017}$	$0.8591^{+0.0089}_{-0.010}$
Ω_m	$0.3088^{+0.0039}_{-0.0095}$	$0.3020^{+0.0045}_{-0.0090}$	$0.2995^{+0.0055}_{-0.0079}$	$0.2999^{+0.0049}_{-0.0089}$	$0.3007^{+0.0046}_{-0.0057}$
$10^2\, a_t$	$3.375^{+0.049}_{-0.21}$	$3.257^{+0.015}_{-0.094}$	$3.275^{+0.014}_{-0.11}$	$3.284^{+0.031}_{-0.12}$	$3.244^{+0.022}_{-0.080}$
Total χ^2	3860.9091	3853.7403	3852.5179	3855.1856	3857.67
$\Delta\chi^2$	6.8811	− 0.2877	− 1.5101	1.1576	3.642

B.3. Planck + Lensing + BAO + SN + H_0 + DES-Y1

See Table 12.

B.4. Planck + Lensing + BAO + SN + H_0 + DES-Y1 + HSC + KIDS

See Table 13.

B.5. Planck + Lensing + BAO + SN + DES-Y1 + HSC + KIDS

See Table 14.

Table 12 The mean $\pm 1\sigma$ constraints on the cosmological parameters inferred from the *Planck* 2018 CMB data (including TTEETE + lensing), BAO, SNe, SH0ES and DES-Y1 for Clustering Emergent DE scenario for different values of n

Constraints from Planck 2018 + Lensing + BAO + SN + H_0 + DES						
Parameter	$n = 1$	$n = 2$	$n = 3$	$n = 4$	$n = 6$	n open
H_0	$67.61^{+0.60}_{-0.29}$	69.00 ± 0.51	$68.88^{+0.48}_{-0.36}$	$68.96^{+0.43}_{-0.27}$	$69.04^{+0.52}_{-0.42}$	$68.93^{+0.50}_{-0.30}$
σ_8	$0.8286^{+0.0061}_{-0.0088}$	$0.8505^{+0.0057}_{-0.0083}$	$0.8463^{+0.0058}_{-0.0072}$	0.8527 ± 0.0075	$0.8534^{+0.0048}_{-0.0075}$	$0.830^{+0.019}_{-0.014}$
S_8	$0.8355^{+0.0082}_{-0.014}$	0.844 ± 0.023	$0.8429^{+0.0078}_{-0.011}$	$0.8478^{+0.0072}_{-0.011}$	$0.8471^{+0.0087}_{-0.011}$	0.825 ± 0.027
Ω_m	$0.3051^{+0.0035}_{-0.0082}$	0.2956 ± 0.0060	$0.2976^{+0.0043}_{-0.0061}$	$0.2966^{+0.0030}_{-0.0056}$	$0.2957^{+0.0049}_{-0.0066}$	$0.2967^{+0.0037}_{-0.0058}$
$10^2\, a_t$	$3.301^{+0.035}_{-0.14}$	$3.228^{+0.011}_{-0.065}$	$3.220^{+0.011}_{-0.058}$	$3.218^{+0.012}_{-0.056}$	$3.221^{+0.011}_{-0.060}$	$3.244^{+0.020}_{-0.081}$
n	1	2	3	4	6	$3.35^{+0.78}_{-0.011}$
Total χ^2	3865.0585	3860.6482	3859.5398	3861.9733	3863.1704	3855.541
$\Delta\chi^2$	9.3301	4.9198	3.8114	6.2449	7.442	0.1874

Table 13 The mean $\pm 1\sigma$ constraints on the cosmological parameters inferred from the *Planck* 2018 CMB data (including TTEETE + lensing), BAO, SNe, SH0ES, DES-Y1 and weak-lensing data for Clustering Emergent DE scenario for different values of n

Constraints from Planck 2018 + Lensing + BAO + SN + H_0 + DES + KIDS + HSC					
Parameter	$n = 1$	$n = 2$	$n = 3$	$n = 4$	$n = 6$
H_0	$67.61^{+0.65}_{-0.43}$	$68.99^{+0.56}_{-0.27}$	$68.98^{+0.66}_{-0.38}$	$69.07^{+0.43}_{-0.39}$	$69.41^{+0.38}_{-0.56}$
σ_8	$0.8242^{+0.0052}_{-0.0083}$	0.844 ± 0.019	0.8418 ± 0.0088	$0.8092^{+0.0056}_{-0.0083}$	$0.8496^{+0.0054}_{-0.0071}$
S_8	$0.8307^{+0.0086}_{-0.015}$	$0.8376^{+0.0070}_{-0.011}$	$0.8364^{+0.0087}_{-0.012}$	$0.8030^{+0.0084}_{-0.011}$	0.837 ± 0.033
Ω_m	$0.3049^{+0.0053}_{-0.0089}$	$0.2956^{+0.0031}_{-0.0070}$	$0.2962^{+0.0045}_{-0.0080}$	$0.2954^{+0.0045}_{-0.0054}$	$0.2909^{+0.0067}_{-0.0046}$
$10^2\, a_t$	$3.260^{+0.018}_{-0.098}$	$3.210^{+0.011}_{-0.049}$	$3.2105^{+0.0096}_{-0.049}$	$3.254^{+0.017}_{-0.091}$	$3.2151^{+0.0054}_{-0.053}$
Total χ^2	3871.3678	3869.4694	3867.4459	3859.2281	3871.5003
$\Delta\chi^2$	11.556	9.6576	7.6341	− 0.5837	11.6885

Table 14 The mean $\pm 1\sigma$ constraints on the cosmological parameters inferred from the *Planck* 2018 CMB data (including TTEETE + lensing), BAO, SNe, DES-Y1 and weak-lensing data for and Clustering Emergent DE scenario for different values of n

Constraints from Planck 2018 + Lensing + BAO + SN + H_0 + DES					
Parameter	$n=1$	$n=2$	$n=3$	$n=4$	$n=6$
H_0	$67.51^{+0.41}_{-0.33}$	$68.87^{+0.44}_{-0.31}$	68.97 ± 0.44	68.82 ± 0.37	$68.90^{+0.46}_{-0.37}$
σ_8	$0.8234^{+0.0059}_{-0.0068}$	$0.8455^{+0.0057}_{-0.010}$	$0.8422^{+0.0052}_{-0.0070}$	$0.8081^{+0.0060}_{-0.0077}$	0.8482 ± 0.0090
S_8	$0.8317^{+0.0074}_{-0.010}$	$0.8413^{+0.0058}_{-0.013}$	$0.8369^{+0.0084}_{-0.0096}$	$0.8059^{+0.0080}_{-0.0098}$	$0.8443^{+0.0074}_{-0.011}$
Ω_m	$0.3061^{+0.0041}_{-0.0057}$	$0.2970^{+0.0038}_{-0.0058}$	$0.2963^{+0.0044}_{-0.0051}$	$0.2984^{+0.0040}_{-0.0048}$	$0.2973^{+0.0043}_{-0.0059}$
$10^2\, a_t$	$3.253^{+0.021}_{-0.091}$	$3.2117^{+0.0082}_{-0.049}$	$3.2071^{+0.0099}_{-0.046}$	$3.241^{+0.030}_{-0.078}$	$3.2060^{+0.0072}_{-0.044}$
Total χ^2	3854.213	3859.4984	3857.8257	3848.0467	3861.4739
$\Delta\chi^2$	8.1357	13.4211	11.7484	1.9694	15.3966

Appendix C. Non canonical emergent dark energy

C.1. Planck TTTEEE only

See Table 15.

C.2. Planck 2018 + Lensing + BAO + SN + H_0

See Table 16.

C.3. Planck + Lensing + BAO + SN + H_0 + DES-Y1

See Table 17.

Table 15 The mean $\pm 1\sigma$ constraints on the cosmological parameters inferred from the *Planck* 2018 CMB data (including TTEETE) data for and Non-canonical Emergent DE scenario for different values of n

Constraints from Planck 2018					
Parameter	$n=1$	$n=2$	$n=3$	$n=4$	$n=6$
H_0	66.18 ± 0.62	68.30 ± 0.70	$68.47^{+0.66}_{-0.74}$	68.48 ± 0.74	68.47 ± 0.77
σ_8	$0.7997^{+0.0077}_{-0.0090}$	$0.8132^{+0.0078}_{-0.0091}$	$0.8147^{+0.0075}_{-0.0098}$	$0.8146^{+0.0077}_{-0.0097}$	$0.8143^{+0.0079}_{-0.0092}$
S_8	0.835 ± 0.017	0.822 ± 0.017	0.821 ± 0.017	0.821 ± 0.017	0.821 ± 0.017
Ω_m	0.3268 ± 0.0091	0.3067 ± 0.0089	0.3050 ± 0.0091	0.3050 ± 0.0092	0.3051 ± 0.0094
$10^2\, a_t$	$3.414^{+0.066}_{-0.25}$	$3.375^{+0.056}_{-0.21}$	$3.372^{+0.053}_{-0.21}$	$3.372^{+0.058}_{-0.21}$	$3.372^{+0.054}_{-0.21}$
c_s^2	$0.64^{+0.29}_{-0.16}$	$0.66^{+0.27}_{-0.16}$	0.65 ± 0.21	$0.65^{+0.28}_{-0.16}$	$0.66^{+0.28}_{-0.15}$
Total χ^2	2765.6229	2766.0841	2765.7061	2765.8519	2765.4524
$\Delta\chi^2$	1.4529	1.9141	1.5361	1.6819	1.2824

Table 16 The mean $\pm 1\sigma$ constraints on the cosmological parameters inferred from the *Planck* 2018 CMB data (including TTEETE + lensing), BAO, SNe, SH0ES data for Non-canonical Emergent DE scenario for different values of n

Constraints from Planck 2018 + Lensing + BAO + SN + H_0					
Parameter	$n=1$	$n=2$	$n=3$	$n=4$	$n=6$
H_0	67.52 ± 0.36	$68.72^{+0.55}_{-0.33}$	$68.83^{+0.44}_{-0.50}$	68.79 ± 0.39	$68.89 \pm 0.53'$
σ_8	$0.8014^{+0.0069}_{-0.0088}$	$0.8154^{+0.0067}_{-0.0086}$	$0.8150^{+0.0065}_{-0.0078}$	$0.8247^{+0.0064}_{-0.0076}$	$0.8155^{+0.0064}_{-0.0080}$
S_8	$0.8121^{+0.0096}_{-0.011}$	$0.8174^{+0.0086}_{-0.014}$	0.816 ± 0.011	0.826 ± 0.013	$0.8156^{+0.0089}_{-0.011}$
Ω_m	0.3081 ± 0.0048	$0.3015^{+0.0038}_{-0.0067}$	0.3007 ± 0.0058	0.3010 ± 0.0045	$0.3001^{+0.0044}_{-0.0055}$
$10^2\, a_t$	$3.502^{+0.097}_{-0.34}$	$3.408^{+0.080}_{-0.24}$	$3.417^{+0.077}_{-0.25}$	$3.405^{+0.083}_{-0.23}$	$3.425^{+0.081}_{-0.26}$
c_s^2	< 0.665	$0.61^{+0.28}_{-0.20}$	$0.66^{+0.23}_{-0.19}$	$0.61^{+0.19}_{-0.25}$	$0.65^{+0.27}_{-0.17}$
Total χ^2	3860.7531	3852.0743	3851.7264	3851.8387	3851.6283
$\Delta\chi^2$	6.7251	− 1.9537	−2.3016	−2.1893	−2.3997

C.4. Planck + Lensing + BAO + SN + H_0 + DES-Y1 + HSC + KIDS

See Table 18.

C.5. Planck + Lensing + BAO + SN + DES-Y1 + HSC + KIDS

See Table 19.

Table 17 The mean $\pm 1\sigma$ constraints on the cosmological parameters inferred from the *Planck* 2018 CMB data (including TTEETE + lensing), BAO, SNe, SH0ES and DES-Y1 data for Non-canonical Emergent DE scenario for different values of n

Constraints from Planck 2018 + Lensing + BAO + SN + H_0 + DES						
Parameter	$n = 1$	$n = 2$	$n = 3$	$n = 4$	$n = 6$	n open
H_0	$67.65^{+0.29}_{-0.43}$	$68.94^{+0.37}_{-0.48}$	$68.93^{+0.44}_{-0.36}$	$69.14^{+0.41}_{-0.56}$	$69.02^{+0.38}_{-0.46}$	68.96 ± 0.40
σ_8	$0.7994^{+0.0061}_{-0.0096}$	$0.8125^{+0.0063}_{-0.0082}$	$0.8129^{+0.0063}_{-0.0085}$	$0.8126^{+0.0061}_{-0.0077}$	$0.8134^{+0.0065}_{-0.0079}$	$0.8125^{+0.0059}_{-0.0079}$
S_8	$0.8078^{+0.0098}_{-0.011}$	0.811 ± 0.011	$0.8119^{+0.0098}_{-0.011}$	$0.8086^{+0.0089}_{-0.010}$	$0.8112^{+0.0087}_{-0.011}$	$0.8108^{+0.0084}_{-0.010}$
Ω_m	$0.3064^{+0.0051}_{-0.0041}$	$0.2988^{+0.0052}_{-0.0046}$	$0.2992^{+0.0042}_{-0.0052}$	$0.2971^{+0.0059}_{-0.0052}$	0.2984 ± 0.0056	0.2988 ± 0.0046
$10^2\, a_t$	$3.510^{+0.088}_{-0.35}$	$3.415^{+0.064}_{-0.25}$	$3.392^{+0.074}_{-0.23}$	$3.447^{+0.092}_{-0.27}$	$3.407^{+0.070}_{-0.24}$	$3.400^{+0.069}_{-0.23}$
c_s^2	0.58 ± 0.23	$0.65^{+0.30}_{-0.14}$	$0.65^{+0.28}_{-0.16}$	$0.69^{+0.20}_{-0.18}$	$0.64^{+0.32}_{-0.14}$	$0.66^{+0.27}_{-0.15}$
n	1	2	3	4	6	> 3.07
Total χ^2	3868.9616	3853.8864	3853.4742	3853.0872	3853.4632	3852.9647
$\Delta\chi^2$	13.2332	-1.842	-2.2542	-2.6412	-2.2652	-2.7637

Table 18 The mean $\pm 1\sigma$ constraints on the cosmological parameters inferred from the *Planck* 2018 CMB data (including TTEETE + lensing), BAO, SNe, SH0ES, DES-Y1 and weak-lensing data for Non-canonical Emergent DE scenario for different values of n

Constraints from Planck 2018 + Lensing + BAO + SN + H_0 + DES + KIDS + HSC					
Parameter	$n = 1$	$n = 2$	$n = 3$	$n = 4$	$n = 6$
H_0	$67.66^{+0.48}_{-0.36}$	69.03 ± 0.70	$69.20^{+0.42}_{-0.54}$	$69.12^{+0.40}_{-0.47}$	$69.24^{+0.27}_{-0.48}$
σ_8	$0.7957^{+0.0058}_{-0.0081}$	$0.8099^{+0.0049}_{-0.0085}$	$0.8126^{+0.0045}_{-0.011}$	$0.8102^{+0.0053}_{-0.0082}$	$0.8103^{+0.0055}_{-0.0083}$
S_8	$0.8037^{+0.0076}_{-0.012}$	$0.8068^{+0.0081}_{-0.010}$	$0.8074^{+0.0072}_{-0.013}$	$0.8060^{+0.0080}_{-0.011}$	0.804 ± 0.010
Ω_m	$0.3061^{+0.0043}_{-0.0062}$	0.2977 ± 0.0074	0.2962 ± 0.0060	0.2969 ± 0.0063	$0.2957^{+0.0053}_{-0.0035}$
$10^2\, a_t$	$3.486^{+0.071}_{-0.32}$	$3.422^{+0.066}_{-0.25}$	$3.454^{+0.072}_{-0.29}$	$3.407^{+0.052}_{-0.24}$	$3.424^{+0.053}_{-0.26}$
c_s^2	$0.59^{+0.20}_{-0.23}$	$0.69^{+0.23}_{-0.15}$	> 0.592	$0.681^{+0.31}_{-0.089}$	$0.69^{+0.29}_{-0.10}$
Total χ^2	3872.2972	3857.2175	3857.2294	3856.8636	3856.7384
$\Delta\chi^2$	12.4852	-2.5943	-2.5824	-2.9482	-3.0734

Table 19 The mean $\pm 1\sigma$ constraints on the cosmological parameters inferred from the *Planck* 2018 CMB data (including TTEETE + lensing), BAO, SNe, DES-Y1 and weak-lensing data for Non-canonical Emergent DE scenario for different values of n

Constraints from Planck 2018 + Lensing + BAO + SN + DES + KIDS + HSC					
Parameter	$n = 1$	$n = 2$	$n = 3$	$n = 4$	$n = 6$
H_0	67.35 ± 0.33	68.69 ± 0.39	68.77 ± 0.38	$68.81^{+0.34}_{-0.40}$	68.79 ± 0.40
σ_8	$0.7947^{+0.0055}_{-0.0071}$	$0.8083^{+0.0054}_{-0.0066}$	$0.8091^{+0.0058}_{-0.0070}$		$0.8091^{+0.0054}_{-0.0068}$
S_8	$0.8076^{+0.0082}_{-0.0093}$	$0.8100^{+0.0080}_{-0.0090}$	$0.8100^{+0.0079}_{-0.0094}$	$0.8111^{+0.0082}_{-0.011}$	$0.8098^{+0.0082}_{-0.0093}$
Ω_m	0.3099 ± 0.0044	0.3013 ± 0.0046	0.3007 ± 0.0045	0.3004 ± 0.0047	0.3006 ± 0.0047
$10^2\, a_t$	$3.419^{+0.068}_{-0.25}$	$3.357^{+0.057}_{-0.19}$	$3.342^{+0.065}_{-0.18}$	$3.350^{+0.047}_{-0.18}$	$3.333^{+0.043}_{-0.17}$
c_s^2	$0.62^{+0.20}_{-0.23}$	> 0.585	$0.68^{+0.25}_{-0.14}$	> 0.582	> 0.595
Total χ^2	3853.5801	3845.4901	3845.5449	3845.2508	3845.3574
$\Delta\chi^2$	7.5028	-0.5872	-0.5324	-0.8265	-0.7199

References

1. Planck Collaboration, N. Aghanim et al., Planck 2018 results. VIII. Gravitational lensing. Astron. Astrophys. **641**, A8 (2020). https://doi.org/10.1051/0004-6361/201833886. arXiv:1807.06210
2. Planck Collaboration, N. Aghanim et al., Planck 2018 results. VI. Cosmological parameters. Astron. Astrophys. **641**, A6 (2020). https://doi.org/10.1051/0004-6361/201833910. arXiv:1807.06209
3. Planck Collaboration, N. Aghanim et al., Planck 2018 results. V. CMB power spectra and likelihoods. Astron. Astrophys. **641**, A5 (2020). https://doi.org/10.1051/0004-6361/201936386. arXiv:1907.12875
4. Pan-STARRS1 Collaboration, D.M. Scolnic et al., The complete light-curve sample of spectroscopically confirmed SNe Ia from Pan-STARRS1 and cosmological constraints from the combined pantheon sample. Astrophys. J. **859**, 101 (2018). https://doi.org/10.3847/1538-4357/aab9bb. arXiv:1710.00845
5. DES Collaboration, T.M.C. Abbott et al., Dark Energy Survey Year 3 results: cosmological constraints from galaxy clustering and weak lensing. Phys. Rev. D **105**, (2022) 023520. https://doi.org/10.1103/PhysRevD.105.023520. arXiv:2105.13549
6. H. Hildebrandt et al., KiDS-450: cosmological parameter constraints from tomographic weak gravitational lensing. Mon. Not. R. Astron. Soc. **465**, 1454 (2017). https://doi.org/10.1093/mnras/stw2805. arXiv:1606.05338
7. H. Hildebrandt et al., KiDS+VIKING-450: cosmic shear tomography with optical and infrared data. Astron. Astrophys. **633**, A69 (2020). https://doi.org/10.1051/0004-6361/201834878. arXiv:1812.06076
8. HSC Collaboration, C. Hikage et al., Cosmology from cosmic shear power spectra with Subaru Hyper Suprime-Cam first-year data. Publ. Astron. Soc. Jpn. **71**, 43 (2019). https://doi.org/10.1093/pasj/psz010. arXiv:1809.09148
9. A.J. Ross, L. Samushia, C. Howlett, W.J. Percival, A. Burden, M. Manera, The clustering of the SDSS DR7 main Galaxy sample—I. A 4 per cent distance measure at $z = 0.15$. Mon. Not. R. Astron. Soc. **449**, 835 (2015). https://doi.org/10.1093/mnras/stv154. arXiv:1409.3242
10. F. Beutler, C. Blake, M. Colless, D.H. Jones, L. Staveley-Smith, L. Campbell et al., The 6dF Galaxy Survey: baryon acoustic oscillations and the local Hubble constant. Mon. Not. R. Astron. Soc. **416**, 3017 (2011). https://doi.org/10.1111/j.1365-2966.2011.19250.x. arXiv:1106.3366
11. BOSS Collaboration, S. Alam et al., The clustering of galaxies in the completed SDSS-III Baryon Oscillation Spectroscopic Survey: cosmological analysis of the DR12 galaxy sample. Mon. Not. R. Astron. Soc. **470**, 2617 (2017). https://doi.org/10.1093/mnras/stx721. arXiv:1607.03155
12. J.E. Bautista et al., The Completed SDSS-IV extended Baryon Oscillation Spectroscopic Survey: measurement of the BAO and growth rate of structure of the luminous red galaxy sample from the anisotropic correlation function between redshifts 0.6 and 1. Mon. Not. R. Astron. Soc. **500**, 736 (2020). https://doi.org/10.1093/mnras/staa2800. arXiv:2007.08993
13. H. Gil-Marin et al., The Completed SDSS-IV extended Baryon Oscillation Spectroscopic Survey: measurement of the BAO and growth rate of structure of the luminous red galaxy sample from the anisotropic power spectrum between redshifts 0.6 and 1.0. Mon. Not. R. Astron. Soc. **498**, 2492 (2020). https://doi.org/10.1093/mnras/staa2455. arXiv:2007.08994
14. eBOSS Collaboration, S. Alam et al., Completed SDSS-IV extended Baryon Oscillation Spectroscopic Survey: cosmological implications from two decades of spectroscopic surveys at the Apache Point Observatory. Phys. Rev. D **103**, 083533 (2021). https://doi.org/10.1103/PhysRevD.103.083533. arXiv:2007.08991
15. R. Neveux et al., The completed SDSS-IV extended Baryon Oscillation Spectroscopic Survey: BAO and RSD measurements from the anisotropic power spectrum of the quasar sample between redshift 0.8 and 2.2. Mon. Not. R. Astron. Soc. **499**, 210 (2020). https://doi.org/10.1093/mnras/staa2780. arXiv:2007.08999
16. J. Hou et al., The Completed SDSS-IV extended Baryon Oscillation Spectroscopic Survey: BAO and RSD measurements from anisotropic clustering analysis of the Quasar Sample in configuration space between redshift 0.8 and 2.2. Mon. Not. R. Astron. Soc. **500**, 1201 (2020). https://doi.org/10.1093/mnras/staa3234. arXiv:2007.08998
17. H. du Mas des Bourboux et al., The Completed SDSS-IV Extended Baryon Oscillation Spectroscopic Survey: baryon acoustic oscillations with Lyα forests. Astrophys. J. **901**, 153 (2020). https://doi.org/10.3847/1538-4357/abb085. arXiv:2007.08995
18. L.A. Escamilla, W. Giarè, E. Di Valentino, R.C. Nunes, S. Vagnozzi, The state of the dark energy equation of state circa 2023. arXiv:2307.14802
19. S. Weinberg, The cosmological constant problem. Rev. Mod. Phys. **61**, 1 (1989). https://doi.org/10.1103/RevModPhys.61.1
20. I. Ben-Dayan, M. Hadad, A. Michaelis, The grand canonical multiverse and the small cosmological constant. JCAP **09**, 052 (2022). https://doi.org/10.1088/1475-7516/2022/09/052. arXiv:2110.06249
21. I. Ben-Dayan, R. Richter, F. Ruehle, A. Westphal, Vacuum energy sequestering and conformal symmetry. JCAP **05**, 002 (2016). https://doi.org/10.1088/1475-7516/2016/05/002. arXiv:1507.04158
22. P.J.E. Peebles, B. Ratra, The cosmological constant and dark energy. Rev. Mod. Phys. **75**, 559 (2003). https://doi.org/10.1103/RevModPhys.75.559. arXiv:astro-ph/0207347
23. S.M. Carroll, W.H. Press, E.L. Turner, The cosmological constant. Annu. Rev. Astron. Astrophys. **30**, 499 (1992). https://doi.org/10.1146/annurev.aa.30.090192.002435
24. S.M. Carroll, The cosmological constant. Living Rev. Relativ. **4**, 1 (2001). https://doi.org/10.12942/lrr-2001-1. arXiv:astro-ph/0004075
25. S. Weinberg, The cosmological constant problems, in *4th International Symposium on Sources and Detection of Dark Matter in the Universe (DM 2000)*, pp. 18–26 (2000). arXiv:astro-ph/0005265
26. V. Sahni, The cosmological constant problem and quintessence. Class. Quantum Gravity **19**, 3435 (2002). https://doi.org/10.1088/0264-9381/19/13/304. arXiv:astro-ph/0202076
27. T. Padmanabhan, Cosmological constant: the weight of the vacuum. Phys. Rep. **380**, 235 (2003). https://doi.org/10.1016/S0370-1573(03)00120-0. arXiv:hep-th/0212290
28. S. Nobbenhuis, Categorizing different approaches to the cosmological constant problem. Found. Phys. **36**, 613 (2006). https://doi.org/10.1007/s10701-005-9042-8. arXiv:gr-qc/0411093
29. J. Polchinski, The cosmological constant and the string landscape, in *23rd Solvay Conference in Physics: The Quantum Structure of Space and Time*, pp. 216–236 (2006). arXiv:hep-th/0603249
30. E.J. Copeland, M. Sami, S. Tsujikawa, Dynamics of dark energy. Int. J. Mod. Phys. D **15**, 1753 (2006). https://doi.org/10.1142/S021827180600942X. arXiv:hep-th/0603057
31. E. Oks, Brief review of recent advances in understanding dark matter and dark energy. New Astron. Rev. **93**, 101632 (2021). https://doi.org/10.1016/j.newar.2021.101632. arXiv:2111.00363
32. D. Huterer et al., Growth of cosmic structure: probing dark energy beyond expansion. Astropart. Phys. **63**, 23 (2015). https://doi.org/10.1016/j.astropartphys.2014.07.004. arXiv:1309.5385

33. G. Caldera-Cabral, R. Maartens, B.M. Schaefer, The growth of structure in interacting dark energy models. JCAP **07**, 027 (2009). https://doi.org/10.1088/1475-7516/2009/07/027. arXiv:0905.0492
34. F. Ferlito, S. Vagnozzi, D.F. Mota, M. Baldi, Cosmological direct detection of dark energy: non-linear structure formation signatures of dark energy scattering with visible matter. Mon. Not. R. Astron. Soc. **512**, 1885 (2022). https://doi.org/10.1093/mnras/stac649. arXiv:2201.04528
35. R.C. Nunes, S. Vagnozzi, Arbitrating the S8 discrepancy with growth rate measurements from redshift-space distortions. Mon. Not. R. Astron. Soc. **505**, 5427 (2021). https://doi.org/10.1093/mnras/stab1613. arXiv:2106.01208
36. M. Chevallier, D. Polarski, Accelerating universes with scaling dark matter. Int. J. Mod. Phys. D **10**, 213 (2001). https://doi.org/10.1142/S0218271801000822. arXiv:gr-qc/0009008
37. E.V. Linder, Exploring the expansion history of the universe. Phys. Rev. Lett. **90**, 091301 (2003). https://doi.org/10.1103/PhysRevLett.90.091301. arXiv:astro-ph/0208512
38. H.K. Jassal, J.S. Bagla, T. Padmanabhan, Observational constraints on low redshift evolution of dark energy: how consistent are different observations? Phys. Rev. D **72**, 103503 (2005). https://doi.org/10.1103/PhysRevD.72.103503. arXiv:astro-ph/0506748
39. E.M. Barboza Jr., J.S. Alcaniz, A parametric model for dark energy. Phys. Lett. B **666**, 415 (2008). https://doi.org/10.1016/j.physletb.2008.08.012. arXiv:0805.1713
40. B.F. Gerke, G. Efstathiou, Probing quintessence: reconstruction and parameter estimation from supernovae. Mon. Not. R. Astron. Soc. **335**, 33 (2002). https://doi.org/10.1046/j.1365-8711.2002.05612.x. arXiv:astro-ph/0201336
41. L.A. Escamilla, O. Akarsu, E. Di Valentino, J.A. Vazquez, Model-independent reconstruction of the interacting dark energy kernel: binned and Gaussian process. arXiv:2305.16290
42. S.A. Adil, M.R. Gangopadhyay, M. Sami, M.K. Sharma, Late-time acceleration due to a generic modification of gravity and the Hubble tension. Phys. Rev. D **104**, 103534 (2021). https://doi.org/10.1103/PhysRevD.104.103534. arXiv:2106.03093
43. A. Aviles, C. Gruber, O. Luongo, H. Quevedo, Cosmography and constraints on the equation of state of the Universe in various parametrizations. Phys. Rev. D **86**, 123516 (2012). https://doi.org/10.1103/PhysRevD.86.123516. arXiv:1204.2007
44. R.K. Sharma, K.L. Pandey, S. Das, Implications of an extended dark energy model with massive neutrinos. Astrophys. J. **934**, 113 (2022). https://doi.org/10.3847/1538-4357/ac7a33. arXiv:2202.01749
45. H.E.S. Velten, R.F. vom Marttens, W. Zimdahl, Aspects of the cosmological "coincidence problem". Eur. Phys. J. C **74**, 3160 (2014). https://doi.org/10.1140/epjc/s10052-014-3160-4. arXiv:1410.2509
46. P.J. Steinhardt, L.-M. Wang, I. Zlatev, Cosmological tracking solutions. Phys. Rev. D **59**, 123504 (1999). https://doi.org/10.1103/PhysRevD.59.123504. arXiv:astro-ph/9812313
47. I. Zlatev, L.-M. Wang, P.J. Steinhardt, Quintessence, cosmic coincidence, and the cosmological constant. Phys. Rev. Lett. **82**, 896 (1999). https://doi.org/10.1103/PhysRevLett.82.896. arXiv:astro-ph/9807002
48. A. Barreira, P.P. Avelino, Anthropic versus cosmological solutions to the coincidence problem. Phys. Rev. D **83**, 103001 (2011). https://doi.org/10.1103/PhysRevD.83.103001. arXiv:1103.2401
49. L. Amendola, Coupled quintessence. Phys. Rev. D **62**, 043511 (2000). https://doi.org/10.1103/PhysRevD.62.043511. arXiv:astro-ph/9908023
50. A.G. Riess et al., A 2.4% determination of the local value of the Hubble constant. Astrophys. J. **826**, 56 (2016). https://doi.org/10.3847/0004-637X/826/1/56. arXiv:1604.01424
51. A.G. Riess, S. Casertano, D. Kenworthy, D. Scolnic, L. Macri, Seven problems with the claims related to the Hubble tension. arXiv:1810.03526
52. A.G. Riess, S. Casertano, W. Yuan, L.M. Macri, D. Scolnic, Large magellanic cloud cepheid standards provide a 1% foundation for the determination of the Hubble constant and stronger evidence for physics beyond ΛCDM. Astrophys. J. **876**, 85 (2019). https://doi.org/10.3847/1538-4357/ab1422. arXiv:1903.07603
53. A.G. Riess, S. Casertano, W. Yuan, J.B. Bowers, L. Macri, J.C. Zinn et al., Cosmic distances calibrated to 1% precision with Gaia EDR3 parallaxes and Hubble space telescope photometry of 75 Milky Way cepheids confirm tension with ΛCDM. Astrophys. J. Lett. **908**, L6 (2021). https://doi.org/10.3847/2041-8213/abdbaf. arXiv:2012.08534
54. A.G. Riess et al., A comprehensive measurement of the local value of the Hubble constant with $1 kms^{-1} Mpc^{-1}$ uncertainty from the Hubble Space Telescope and the SH0ES Team. Astrophys. J. Lett. **934**, L7 (2022). https://doi.org/10.3847/2041-8213/ac5c5b. arXiv:2112.04510
55. W.L. Freedman, Cosmology at a crossroads. Nat. Astron. **1**, 0121 (2017). https://doi.org/10.1038/s41550-017-0121. arXiv:1706.02739
56. W.L. Freedman et al., The Carnegie-Chicago Hubble Program. VIII. An independent determination of the Hubble constant based on the tip of the Red Giant Branch. Astrophys. J. **882**, 34 (2019). https://doi.org/10.3847/1538-4357/ab2f73. arXiv:1907.05922
57. W.L. Freedman, B.F. Madore, T. Hoyt, I.S. Jang, R. Beaton, M.G. Lee et al., Calibration of the Tip of the Red Giant Branch (TRGB). arXiv:2002.01550
58. W.L. Freedman, Measurements of the Hubble constant: tensions in perspective. Astrophys. J. **919**, 16 (2021). https://doi.org/10.3847/1538-4357/ac0e95. arXiv:2106.15656
59. D. Camarena, V. Marra, The tension in the absolute magnitude of Type Ia supernovae. arXiv:2307.02434
60. D. Camarena, V. Marra, A new method to build the (inverse) distance ladder. Mon. Not. R. Astron. Soc. **495**, 2630 (2020). https://doi.org/10.1093/mnras/staa770. arXiv:1910.14125
61. D. Camarena, V. Marra, Impact of the cosmic variance on H_0 on cosmological analyses. Phys. Rev. D **98**, 023537 (2018). https://doi.org/10.1103/PhysRevD.98.023537. arXiv:1805.09900
62. D. Camarena, V. Marra, Local determination of the Hubble constant and the deceleration parameter. Phys. Rev. Res. **2**, 013028 (2020). https://doi.org/10.1103/PhysRevResearch.2.013028. arXiv:1906.11814
63. A. Aviles, J. Klapp, O. Luongo, Toward unbiased estimations of the statefinder parameters. Phys. Dark Univ. **17**, 25 (2017). https://doi.org/10.1016/j.dark.2017.07.002. arXiv:1606.09195
64. L. Verde, T. Treu, A.G. Riess, Tensions between the Early and the Late Universe. Nat. Astron. **3**, 891 (2019). https://doi.org/10.1038/s41550-019-0902-0. arXiv:1907.10625
65. E. Di Valentino et al., Cosmology intertwined III: $f\sigma_8$ and S_8. Astropart. Phys. **131**, 102604 (2021). https://doi.org/10.1016/j.astropartphys.2021.102604. arXiv:2008.11285
66. M. White et al., Cosmological constraints from the tomographic cross-correlation of DESI Luminous Red Galaxies and Planck CMB lensing. JCAP **02**, 007 (2022). https://doi.org/10.1088/1475-7516/2022/02/007. arXiv:2111.09898
67. C. Heymans et al., KiDS-1000 cosmology: multi-probe weak gravitational lensing and spectroscopic galaxy clustering constraints. Astron. Astrophys. **646**, A140 (2021). https://doi.org/10.1051/0004-6361/202039063. arXiv:2007.15632
68. DES Collaboration, S. Pandey et al., Dark Energy Survey year 3 results: constraints on cosmological parameters and galaxy-bias models from galaxy clustering and galaxy-galaxy lensing using the redMaGiC sample. Phys. Rev. D **106**, 043520. (2022) https://doi.org/10.1103/PhysRevD.106.043520. arXiv:2105.13545

69. C. García-García, J.R. Zapatero, D. Alonso, E. Bellini, P.G. Ferreira, E.-M. Mueller et al., The growth of density perturbations in the last ∼10 billion years from tomographic large-scale structure data. JCAP **10**, 030 (2021). https://doi.org/10.1088/1475-7516/2021/10/030. arXiv:2105.12108
70. LSST Dark Energy Science Collaboration, E.P. Longley et al., A unified catalog-level reanalysis of stage-III cosmic shear surveys. arXiv:2208.07179
71. ACT Collaboration, S. Aiola et al., The Atacama Cosmology Telescope: DR4 Maps and Cosmological Parameters. arXiv:2007.07288
72. S.-F. Chen, M. White, J. DeRose, N. Kokron, Cosmological analysis of three-dimensional BOSS galaxy clustering and Planck CMB lensing cross correlations via Lagrangian perturbation theory. JCAP **07**, 041 (2022). https://doi.org/10.1088/1475-7516/2022/07/041. arXiv:2204.10392
73. D. Brout et al., The Pantheon+ Analysis: Cosmological Constraints. arXiv:2202.04077
74. E. Mörtsell, S. Dhawan, Does the Hubble constant tension call for new physics? JCAP **09**, 025 (2018). https://doi.org/10.1088/1475-7516/2018/09/025. arXiv:1801.07260
75. M. Kamionkowski, A.G. Riess, The Hubble Tension and Early Dark Energy. arXiv:2211.04492
76. P. Agrawal, F.-Y. Cyr-Racine, D. Pinner, L. Randall, Rock 'n' Roll Solutions to the Hubble Tension. arXiv:1904.01016
77. M.-X. Lin, G. Benevento, W. Hu, M. Raveri, Acoustic dark energy: potential conversion of the Hubble tension. Phys. Rev. D **100**, 063542 (2019). https://doi.org/10.1103/PhysRevD.100.063542. arXiv:1905.12618
78. T.L. Smith, V. Poulin, M.A. Amin, Oscillating scalar fields and the Hubble tension: a resolution with novel signatures. Phys. Rev. D **101**, 063523 (2020). https://doi.org/10.1103/PhysRevD.101.063523. arXiv:1908.06995
79. S. Alexander, H. Bernardo, M.W. Toomey, Addressing the Hubble and S_8 Tensions with a Kinetically Mixed Dark Sector. arXiv:2207.13086
80. L. Knox, M. Millea, Hubble constant hunter's guide. Phys. Rev. D **101**, 043533 (2020). https://doi.org/10.1103/PhysRevD.101.043533. arXiv:1908.03663
81. V.I. Sabla, R.R. Caldwell, No H_0 assistance from assisted quintessence. Phys. Rev. D **103**, 103506 (2021). https://doi.org/10.1103/PhysRevD.103.103506. arXiv:2103.04999
82. J. Sakstein, M. Trodden, Early dark energy from massive neutrinos as a natural resolution of the Hubble tension. Phys. Rev. Lett. **124**, 161301 (2020). https://doi.org/10.1103/PhysRevLett.124.161301. arXiv:1911.11760
83. M. Carrillo González, Q. Liang, J. Sakstein, M. Trodden, Neutrino-assisted early dark energy: theory and cosmology. JCAP **04**, 063 (2021). https://doi.org/10.1088/1475-7516/2021/04/063. arXiv:2011.09895
84. J.C. Hill, E. McDonough, M.W. Toomey, S. Alexander, Early dark energy does not restore cosmological concordance. Phys. Rev. D **102**, 043507 (2020). https://doi.org/10.1103/PhysRevD.102.043507. arXiv:2003.07355
85. M.M. Ivanov, E. McDonough, J.C. Hill, M. Simonović, M.W. Toomey, S. Alexander et al., Constraining early dark energy with large-scale structure. Phys. Rev. D **102**, 103502 (2020). https://doi.org/10.1103/PhysRevD.102.103502. arXiv:2006.11235
86. E. Di Valentino, S. Bridle, Exploring the tension between current cosmic microwave background and cosmic shear data. Symmetry **10**, 585 (2018). https://doi.org/10.3390/sym10110585
87. A. Cuceu, J. Farr, P. Lemos, A. Font-Ribera, Baryon acoustic oscillations and the Hubble constant: past, present and future. JCAP **10**, 044 (2019). https://doi.org/10.1088/1475-7516/2019/10/044. arXiv:1906.11628
88. N. Schöneberg, J. Lesgourgues, D.C. Hooper, The BAO+BBN take on the Hubble tension. JCAP **10**, 029 (2019). https://doi.org/10.1088/1475-7516/2019/10/029. arXiv:1907.11594
89. A. Krolewski, S. Ferraro, The Integrated Sachs Wolfe effect: unWISE and Planck constraints on dynamical dark energy. JCAP **04**, 033 (2022). https://doi.org/10.1088/1475-7516/2022/04/033. arXiv:2110.13959
90. S. Vagnozzi, New physics in light of the H_0 tension: an alternative view. Phys. Rev. D **102**, 023518 (2020). https://doi.org/10.1103/PhysRevD.102.023518. arXiv:1907.07569
91. S. Vagnozzi, A. Loeb, M. Moresco, Eppur è piatto? The cosmic chronometers take on spatial curvature and cosmic concordance. Astrophys. J. **908**, 84 (2021). https://doi.org/10.3847/1538-4357/abd4df. arXiv:2011.11645
92. S. Vagnozzi, Consistency tests of ΛCDM from the early integrated Sachs–Wolfe effect: implications for early-time new physics and the Hubble tension. Phys. Rev. D **104**, 063524 (2021). https://doi.org/10.1103/PhysRevD.104.063524. arXiv:2105.10425
93. S. Vagnozzi, F. Pacucci, A. Loeb, Implications for the Hubble tension from the ages of the oldest astrophysical objects. JHEAp **36**, 27 (2022). https://doi.org/10.1016/j.jheap.2022.07.004. arXiv:2105.10421
94. L. Feng, J.-F. Zhang, X. Zhang, A search for sterile neutrinos with the latest cosmological observations. Eur. Phys. J. C **77**, 418 (2017). https://doi.org/10.1140/epjc/s10052-017-4986-3. arXiv:1703.04884
95. M. Benetti, L.L. Graef, J.S. Alcaniz, Do joint CMB and HST data support a scale invariant spectrum? JCAP **04**, 003 (2017). https://doi.org/10.1088/1475-7516/2017/04/003. arXiv:1702.06509
96. S. Kumar, R.C. Nunes, Echo of interactions in the dark sector. Phys. Rev. D **96**, 103511 (2017). https://doi.org/10.1103/PhysRevD.96.103511. arXiv:1702.02143
97. S. Vagnozzi, E. Giusarma, O. Mena, K. Freese, M. Gerbino, S. Ho et al., Unveiling ν secrets with cosmological data: neutrino masses and mass hierarchy. Phys. Rev. D **96**, 123503 (2017). https://doi.org/10.1103/PhysRevD.96.123503. arXiv:1701.08172
98. G.-B. Zhao et al., Dynamical dark energy in light of the latest observations. Nat. Astron. **1**, 627 (2017). https://doi.org/10.1038/s41550-017-0216-z. arXiv:1701.08165
99. V. Prilepina, Y. Tsai, Reconciling large and small-scale structure in twin Higgs models. JHEP **09**, 033 (2017). https://doi.org/10.1007/JHEP09(2017)033. arXiv:1611.05879
100. Z. Chacko, Y. Cui, S. Hong, T. Okui, Y. Tsai, Partially acoustic dark matter, interacting dark radiation, and large scale structure. JHEP **12**, 108 (2016). https://doi.org/10.1007/JHEP12(2016)108. arXiv:1609.03569
101. P. Ko, Y. Tang, Residual non-abelian dark matter and dark radiation. Phys. Lett. B **768**, 12 (2017). https://doi.org/10.1016/j.physletb.2017.02.033. arXiv:1609.02307
102. D.-M. Xia, S. Wang, Constraining interacting dark energy models with latest cosmological observations. Mon. Not. R. Astron. Soc. **463**, 952 (2016). https://doi.org/10.1093/mnras/stw2073. arXiv:1608.04545
103. S. Kumar, R.C. Nunes, Probing the interaction between dark matter and dark energy in the presence of massive neutrinos. Phys. Rev. D **94**, 123511 (2016). https://doi.org/10.1103/PhysRevD.94.123511. arXiv:1608.02454
104. T. Karwal, M. Kamionkowski, Dark energy at early times, the Hubble parameter, and the string axiverse. Phys. Rev. D **94**, 103523 (2016). https://doi.org/10.1103/PhysRevD.94.103523. arXiv:1608.01309
105. P. Ko, Y. Tang, Light dark photon and fermionic dark radiation for the Hubble constant and the structure formation. Phys. Lett. B **762**, 462 (2016). https://doi.org/10.1016/j.physletb.2016.10.001. arXiv:1608.01083

106. T. Tram, R. Vallance, V. Vennin, Inflation model selection meets dark radiation. JCAP **01**, 046 (2017). https://doi.org/10.1088/1475-7516/2017/01/046. arXiv:1606.09199
107. Q.-G. Huang, K. Wang, How the dark energy can reconcile Planck with local determination of the Hubble constant. Eur. Phys. J. C **76**, 506 (2016). https://doi.org/10.1140/epjc/s10052-016-4352-x. arXiv:1606.05965
108. E. Di Valentino, A. Melchiorri, J. Silk, Reconciling Planck with the local value of H_0 in extended parameter space. Phys. Lett. B **761**, 242 (2016). https://doi.org/10.1016/j.physletb.2016.08.043. arXiv:1606.00634
109. J. Solà Peracaula, J. de Cruz Pérez, A. Gómez-Valent, Dynamical dark energy vs. Λ = const in light of observations. EPL **121**, 39001 (2018). https://doi.org/10.1209/0295-5075/121/39001. arXiv:1606.00450
110. J. Solà, A. Gómez-Valent, J. de Cruz Pérez, First evidence of running cosmic vacuum: challenging the concordance model. Astrophys. J. **836**, 43 (2017). https://doi.org/10.3847/1538-4357/836/1/43. arXiv:1602.02103
111. J. Sola, A. Gomez-Valent, J. de Cruz Pérez, Hints of dynamical vacuum energy in the expanding Universe. Astrophys. J. Lett. **811**, L14 (2015). https://doi.org/10.1088/2041-8205/811/1/L14. arXiv:1506.05793
112. Z. Berezhiani, A.D. Dolgov, I.I. Tkachev, Reconciling Planck results with low redshift astronomical measurements. Phys. Rev. D **92**, 061303 (2015). https://doi.org/10.1103/PhysRevD.92.061303. arXiv:1505.03644
113. R. Wojtak, J. Hjorth, Intrinsic tension in the supernova sector of the local Hubble constant measurement and its implications. Mon. Not. R. Astron. Soc. **515**, 2790 (2022). https://doi.org/10.1093/mnras/stac1878. arXiv:2206.08160
114. E. Mortsell, A. Goobar, J. Johansson, S. Dhawan, The Hubble tension revisited: additional local distance ladder uncertainties. Astrophys. J. **935**, 58 (2022). https://doi.org/10.3847/1538-4357/ac7c19. arXiv:2106.09400
115. E. Mortsell, A. Goobar, J. Johansson, S. Dhawan, Sensitivity of the Hubble constant determination to Cepheid calibration. Astrophys. J. **933**, 212 (2022). https://doi.org/10.3847/1538-4357/ac756e. arXiv:2105.11461
116. G. Efstathiou, A lockdown perspective on the Hubble tension (with comments from the SH0ES team). arXiv:2007.10716
117. J.-P. Hu, F.-Y. Wang, Hubble tension: the evidence of new physics. Universe **9**, 94 (2023). https://doi.org/10.3390/universe9020094. arXiv:2302.05709
118. E. Di Valentino, Challenges of the standard cosmological model. Universe **8**, 399 (2022). https://doi.org/10.3390/universe8080399
119. E. Abdalla et al., Cosmology intertwined: a review of the particle physics, astrophysics, and cosmology associated with the cosmological tensions and anomalies. JHEAP **34**, 49 (2022). https://doi.org/10.1016/j.jheap.2022.04.002. arXiv:2203.06142
120. P. Shah, P. Lemos, O. Lahav, A buyer's guide to the Hubble constant. Astron. Astrophys. Rev. **29**, 9 (2021). https://doi.org/10.1007/s00159-021-00137-4. arXiv:2109.01161
121. L. Perivolaropoulos, F. Skara, Challenges for ΛCDM: an update. New Astron. Rev. **95**, 101659 (2022). https://doi.org/10.1016/j.newar.2022.101659. arXiv:2105.05208
122. E. Di Valentino, O. Mena, S. Pan, L. Visinelli, W. Yang, A. Melchiorri et al., In the realm of the Hubble tension—a review of solutions. Class. Quantum Gravity **38**, 153001 (2021). https://doi.org/10.1088/1361-6382/ac086d. arXiv:2103.01183
123. E. Di Valentino et al., Snowmass 2021—Letter of interest cosmology intertwined II: the Hubble constant tension. Astropart. Phys. **131**, 102605 (2021). https://doi.org/10.1016/j.astropartphys.2021.102605. arXiv:2008.11284
124. E. Di Valentino, A. Melchiorri, O. Mena, S. Vagnozzi, Interacting dark energy in the early 2020s: a promising solution to the H_0 and cosmic shear tensions. Phys. Dark Univ. **30**, 100666 (2020). https://doi.org/10.1016/j.dark.2020.100666. arXiv:1908.04281
125. E. Di Valentino, A. Melchiorri, O. Mena, S. Vagnozzi, Nonminimal dark sector physics and cosmological tensions. Phys. Rev. D **101**, 063502 (2020). https://doi.org/10.1103/PhysRevD.101.063502. arXiv:1910.09853
126. S. Dhawan, J. Alsing, S. Vagnozzi, Non-parametric spatial curvature inference using late-Universe cosmological probes. Mon. Not. R. Astron. Soc. **506**, L1 (2021). https://doi.org/10.1093/mnrasl/slab058. arXiv:2104.02485
127. O.H.E. Philcox, M.M. Ivanov, BOSS DR12 full-shape cosmology: ΛCDM constraints from the large-scale galaxy power spectrum and bispectrum monopole. Phys. Rev. D **105**, 043517 (2022). https://doi.org/10.1103/PhysRevD.105.043517. arXiv:2112.04515
128. P. Zhang, G. D'Amico, L. Senatore, C. Zhao, Y. Cai, BOSS correlation function analysis from the effective field theory of large-scale structure. JCAP **02**, 036 (2022). https://doi.org/10.1088/1475-7516/2022/02/036. arXiv:2110.07539
129. S. Yuan, L.H. Garrison, D.J. Eisenstein, R.H. Wechsler, Stringent $\sigma 8$ constraints from small-scale galaxy clustering using a hybrid MCMC + emulator framework. Mon. Not. R. Astron. Soc. **515**, 871 (2022). https://doi.org/10.1093/mnras/stac1830. arXiv:2203.11963
130. Z. Zhai, J.L. Tinker, A. Banerjee, J. DeRose, H. Guo, Y.-Y. Mao et al., The Aemulus Project V: cosmological constraint from small-scale clustering of BOSS galaxies. arXiv:2203.08999
131. T. Simon, P. Zhang, V. Poulin, T.L. Smith, On the consistency of effective field theory analyses of BOSS power spectrum. arXiv:2208.05929
132. DES Collaboration, A. Amon et al., Dark Energy Survey Year 3 results: cosmology from cosmic shear and robustness to data calibration. Phys. Rev. D **105**, 023514 (2022). https://doi.org/10.1103/PhysRevD.105.023514. arXiv:2105.13543
133. J.L.D. Busch et al., KiDS-1000: cosmic shear with enhanced redshift calibration. arXiv:2204.02396
134. Planck Collaboration, P.A.R. Ade et al., Planck 2015 results. XXIV. Cosmology from Sunyaev–Zeldovich cluster counts. Astron. Astrophys. **594**, A24 (2016). https://doi.org/10.1051/0004-6361/201525833. arXiv:1502.01597
135. A. Krolewski, S. Ferraro, M. White, Cosmological constraints from unWISE and Planck CMB lensing tomography. JCAP **12**, 028 (2021). https://doi.org/10.1088/1475-7516/2021/12/028. arXiv:2105.03421
136. N. Schöneberg, G. Franco Abellán, A. Pérez Sánchez, S. J. Witte, V. Poulin, J. Lesgourgues, The H0 Olympics: a fair ranking of proposed models. Phys. Rep. **984**, 1 (2022). https://doi.org/10.1016/j.physrep.2022.07.001. arXiv:2107.10291
137. A. Amon, G. Efstathiou, A non-linear solution to the S_8 tension?. arXiv:2206.11794
138. A. Sarkar, B. Ghosh, Early Dark Energy Motivated Quintessential α-Attractor Inflaton Potential. arXiv:2307.00603
139. A. Sarkar, B. Ghosh, Constraining the quintessential α-attractor inflation through dynamical horizon exit method. Phys. Dark Univ. **41**, 101239 (2023). https://doi.org/10.1016/j.dark.2023.101239. arXiv:2305.00230
140. G. Bargiacchi, M.G. Dainotti, S. Capozziello, Tensions with the flat ΛCDM model from high-redshift cosmography. arXiv:2307.15359
141. M.G. Dainotti, G. Bargiacchi, M. Bogdan, A.L. Lenart, K. Iwasaki, S. Capozziello et al., Reducing the uncertainty on the Hubble constant up to 35% with an improved statistical analysis: different best-fit likelihoods for type Ia supernovae, baryon acoustic oscillations, quasars, and gamma-ray bursts. Astrophys. J. **951**, 63 (2023). https://doi.org/10.3847/1538-4357/acd63f. arXiv:2305.10030

142. G. Bargiacchi, M. Benetti, S. Capozziello, E. Lusso, G. Risaliti, M. Signorini, Quasar cosmology: dark energy evolution and spatial curvature. Mon. Not. R. Astron. Soc. **515**, 1795 (2022). https://doi.org/10.1093/mnras/stac1941. arXiv:2111.02420
143. G. Bargiacchi, M.G. Dainotti, S. Nagataki, S. Capozziello, Gamma-Ray Bursts, Quasars, Baryonic Acoustic Oscillations, and Supernovae Ia: new statistical insights and cosmological constraints. arXiv:2303.07076
144. A.L. Lenart, G. Bargiacchi, M.G. Dainotti, S. Nagataki, S. Capozziello, A bias-free cosmological analysis with quasars alleviating H $_0$ tension. Astrophys. J. Suppl. **264**, 46 (2023). https://doi.org/10.3847/1538-4365/aca404. arXiv:2211.10785
145. M.G. Dainotti, B. De Simone, T. Schiavone, G. Montani, E. Rinaldi, G. Lambiase et al., On the evolution of the Hubble constant with the SNe Ia pantheon sample and baryon acoustic oscillations: a feasibility study for GRB-cosmology in 2030. Galaxies **10**, 24 (2022). https://doi.org/10.3390/galaxies10010024. arXiv:2201.09848
146. M.G. Dainotti, B. De Simone, T. Schiavone, G. Montani, E. Rinaldi, G. Lambiase, On the Hubble constant tension in the SNe Ia Pantheon sample. Astrophys. J. **912**, 150 (2021). https://doi.org/10.3847/1538-4357/abeb73. arXiv:2103.02117
147. M.G. Dainotti, G. Bargiacchi, M. Bogdan, S. Capozziello, S. Nagataki, Reduced uncertainties up to 43% on the Hubble constant and the matter density with the SNe Ia with a new statistical analysis. arXiv:2303.06974
148. A. Reeves, L. Herold, S. Vagnozzi, B.D. Sherwin, E.G.M. Ferreira, Restoring cosmological concordance with early dark energy and massive neutrinos? Mon. Not. R. Astron. Soc. **520**, 3688 (2023). https://doi.org/10.1093/mnras/stad317. arXiv:2207.01501
149. I. Ben-Dayan, U. Kumar, Emergent Unparticles Dark Energy can restore cosmological concordance. arXiv:2302.00067
150. M. Artymowski, I. Ben-Dayan, U. Kumar, More on emergent dark energy from unparticles. Phys. Rev. D **106**, 083502 (2022). https://doi.org/10.1103/PhysRevD.106.083502. arXiv:2111.09946
151. M. Artymowski, I. Ben-Dayan, U. Kumar, Emergent dark energy from unparticles. Phys. Rev. D **103**, L121303 (2021). https://doi.org/10.1103/PhysRevD.103.L121303. arXiv:2010.02998
152. P. Agrawal, G. Obied, C. Vafa, H_0 tension, swampland conjectures, and the epoch of fading dark matter. Phys. Rev. D **103**, 043523 (2021). https://doi.org/10.1103/PhysRevD.103.043523. arXiv:1906.08261
153. C. Vafa, The String landscape and the swampland. arXiv:hep-th/0509212
154. E. Palti, The Swampland: introduction and review. Fortsch. Phys. **67**, 1900037 (2019). https://doi.org/10.1002/prop.201900037. arXiv:1903.06239
155. G. Obied, H. Ooguri, L. Spodyneiko, C. Vafa, De Sitter Space and the Swampland. arXiv:1806.08362
156. P. Agrawal, G. Obied, P.J. Steinhardt, C. Vafa, On the cosmological implications of the string Swampland. Phys. Lett. B **784**, 271 (2018). https://doi.org/10.1016/j.physletb.2018.07.040. arXiv:1806.09718
157. S.K. Garg, C. Krishnan, Bounds on slow roll and the de Sitter Swampland. JHEP **11**, 075 (2019). https://doi.org/10.1007/JHEP11(2019)075. arXiv:1807.05193
158. H. Ooguri, E. Palti, G. Shiu, C. Vafa, Distance and de Sitter conjectures on the Swampland. Phys. Lett. B **788**, 180 (2019). https://doi.org/10.1016/j.physletb.2018.11.018. arXiv:1810.05506
159. I. Ben-Dayan, Draining the Swampland. Phys. Rev. D **99**, 101301 (2019). https://doi.org/10.1103/PhysRevD.99.101301. arXiv:1808.01615
160. E. Frion, D. Camarena, L. Giani, T. Miranda, D. Bertacca, V. Marra et al., Bayesian analysis of Unified Dark Matter models with fast transition: can they alleviate the H_0 tension?. arXiv:2307.06320
161. R. Lazkoz, I. Leanizbarrutia, V. Salzano, Cosmological constraints on fast transition unified dark energy and dark matter models. Phys. Rev. D **93**, 043537 (2016). https://doi.org/10.1103/PhysRevD.93.043537. arXiv:1602.01331
162. I. Leanizbarrutia, A. Rozas-Fernández, I. Tereno, Cosmological constraints on a unified dark matter-energy scalar field model with fast transition. Phys. Rev. D **96**, 023503 (2017). https://doi.org/10.1103/PhysRevD.96.023503. arXiv:1706.01706
163. C.J.A.P. Martins, M.P. Colomer, Constraining late-time transitions in the dark energy equation of state. Astron. Astrophys. **616**, A32 (2018). https://doi.org/10.1051/0004-6361/201833313. arXiv:1806.07653
164. C.-P. Ma, E. Bertschinger, Cosmological perturbation theory in the synchronous and conformal Newtonian gauges. Astrophys. J. **455**, 7 (1995). https://doi.org/10.1086/176550. arXiv:astro-ph/9506072
165. J.M. Bardeen, Gauge-invariant cosmological perturbations. Phys. Rev. D **22**, 1882 (1980). https://doi.org/10.1103/PhysRevD.22.1882
166. M. Raveri, W. Hu, Concordance and discordance in cosmology. Phys. Rev. D **99**, 043506 (2019). https://doi.org/10.1103/PhysRevD.99.043506. arXiv:1806.04649
167. Kilo-Degree Survey, DES Collaboration, T.M.C. Abbott et al., DES Y3 + KiDS-1000: consistent cosmology combining cosmic shear surveys. arXiv:2305.17173
168. T. Barreiro, E.J. Copeland, N.J. Nunes, Quintessence arising from exponential potentials. Phys. Rev. D **61**, 127301 (2000). https://doi.org/10.1103/PhysRevD.61.127301. arXiv:astro-ph/9910214
169. T. Chiba, A. De Felice, S. Tsujikawa, Observational constraints on quintessence: thawing, tracker, and scaling models. Phys. Rev. D **87**, 083505 (2013). https://doi.org/10.1103/PhysRevD.87.083505. arXiv:1210.3859
170. R.R. Caldwell, M. Doran, C.M. Mueller, G. Schafer, C. Wetterich, Early quintessence in light of WMAP. Astrophys. J. Lett. **591**, L75 (2003). https://doi.org/10.1086/376975. arXiv:astro-ph/0302505
171. R.R. Caldwell, An introduction to quintessence. Braz. J. Phys. **30**, 215 (2000). https://doi.org/10.1590/S0103-97332000000200002
172. R.R. Caldwell, M. Doran, Cosmic microwave background and supernova constraints on quintessence: concordance regions and target models. Phys. Rev. D **69**, 103517 (2004). https://doi.org/10.1103/PhysRevD.69.103517. arXiv:astro-ph/0305334
173. A. Guarnizo, J.B. Orjuela-Quintana, C.A. Valenzuela-Toledo, Dynamical analysis of cosmological models with non-Abelian gauge vector fields. Phys. Rev. D **102**, 083507 (2020). https://doi.org/10.1103/PhysRevD.102.083507. arXiv:2007.12964
174. A. Mehrabi, A. Maleknejad, V. Kamali, Gaugessence: a dark energy model with early time radiation-like equation of state. Astrophys. Space Sci. **362**, 53 (2017). https://doi.org/10.1007/s10509-017-3033-z. arXiv:1510.00838
175. L.G. Gomez, Y. Rodriguez, Coupled multi-Proca vector dark energy. Phys. Dark Univ. **31**, 100759 (2021). https://doi.org/10.1016/j.dark.2020.100759. arXiv:2004.06466
176. R.C. Batista, A short review on clustering dark energy. Universe **8**, 22 (2021). https://doi.org/10.3390/universe8010022. arXiv:2204.12341
177. J. Dakin, S. Hannestad, T. Tram, M. Knabenhans, J. Stadel, Dark energy perturbations in N-body simulations. JCAP **08**, 013 (2019). https://doi.org/10.1088/1475-7516/2019/08/013. arXiv:1904.05210
178. F. Hassani, J. Adamek, M. Kunz, F. Vernizzi, k-evolution: a relativistic N-body code for clustering dark energy. JCAP **12**, 011 (2019). https://doi.org/10.1088/1475-7516/2019/12/011. arXiv:1910.01104

179. F. Hassani, J. Adamek, M. Kunz, Clustering dark energy imprints on cosmological observables of the gravitational field. Mon. Not. R. Astron. Soc. **500**, 4514 (2020). https://doi.org/10.1093/mnras/staa3589. arXiv:2007.04968
180. D.F. Mota, C. van de Bruck, On the spherical collapse model in dark energy cosmologies. Astron. Astrophys. **421**, 71 (2004). https://doi.org/10.1051/0004-6361:20041090. arXiv:astro-ph/0401504
181. D. Bertacca, N. Bartolo, A. Diaferio, S. Matarrese, How the scalar field of unified dark matter models can cluster. JCAP **10**, 023 (2008). https://doi.org/10.1088/1475-7516/2008/10/023. arXiv:0807.1020
182. C. Armendariz-Picon, V.F. Mukhanov, P.J. Steinhardt, Essentials of k essence. Phys. Rev. D **63**, 103510 (2001). https://doi.org/10.1103/PhysRevD.63.103510. arXiv:astro-ph/0006373
183. A. Joseph, R. Saha, Dark energy with oscillatory tracking potential: observational constraints and perturbative effects. Mon. Not. R. Astron. Soc. **511**, 1637 (2022). https://doi.org/10.1093/mnras/stac201. arXiv:2110.00229
184. S. DeDeo, R.R. Caldwell, P.J. Steinhardt, Effects of the sound speed of quintessence on the microwave background and large scale structure. Phys. Rev. D **67**, 103509 (2003). https://doi.org/10.1103/PhysRevD.67.103509. arXiv:astro-ph/0301284
185. J.K. Erickson, R.R. Caldwell, P.J. Steinhardt, C. Armendariz-Picon, V.F. Mukhanov, Measuring the speed of sound of quintessence. Phys. Rev. Lett. **88**, 121301 (2002). https://doi.org/10.1103/PhysRevLett.88.121301. arXiv:astro-ph/0112438
186. R. D'Agostino, O. Luongo, M. Muccino, Healing the cosmological constant problem during inflation through a unified quasi-quintessence matter field. Class. Quantum Gravity **39**, 195014 (2022). https://doi.org/10.1088/1361-6382/ac8af2. arXiv:2204.02190
187. O. Luongo, H. Quevedo, A unified dark energy model from a vanishing speed of sound with emergent cosmological constant. Int. J. Mod. Phys. D **23**, 1450012 (2014). https://doi.org/10.1142/S0218271814500126
188. J. Torrado, A. Lewis, Cobaya: code for Bayesian analysis of hierarchical physical models. JCAP **05**, 057 (2021). https://doi.org/10.1088/1475-7516/2021/05/057. arXiv:2005.05290
189. A. Lewis, A. Challinor, A. Lasenby, Efficient computation of CMB anisotropies in closed FRW models. Astrophys. J. **538**, 473 (2000). https://doi.org/10.1086/309179. arXiv:astro-ph/9911177
190. A. Gelman, D.B. Rubin, Inference from iterative simulation using multiple sequences. Statist. Sci. **7**, 457 (1992). https://doi.org/10.1214/ss/1177011136